ACS APPLIED MATERIALS & INTERFACES

www.acsami.org

Research Article

Albendazole Nanocrystal-Based Dissolving Microneedles with Improved Pharmacokinetic Performance for Enhanced Treatment of Cystic Echinococcosis

Andi Dian Permana, Alejandro J. Paredes, Fabiana Volpe Zanutto, Muh. Nur Amir, Ismail Ismail, Muh. Akbar Bahar, Sumarheni, Santiago Daniel Palma, and Ryan F. Donnelly*

Cite This: https://doi.org/10.1021/acsami.1c11179

Read Online

ACCESS | Metrics & More | Article Recommendations

ABSTRACT: Cystic echinococcosis (CE) is a zoonosis caused by *Echinococcus* spp., affecting both humans and animals' lives. Current treatment of CE by oral administration of albendazole (ABZ) is hampered by several limitations. The poor aqueous solubility and the rapid metabolism of ABZ in the liver are the main issues, leading to lack of efficacy of the treatment. In the present study, we developed a nanocrystalline (NC) formulation of ABZ to be delivered intradermally using dissolving microneedles (DMNs). The NC formulation was developed using milling in an ultrasmall-scale device. Following several screenings, Pluronic F127 was selected as a suitable stabilizer, producing NCs with around 400 nm in size with narrow particle distribution. The crystallinity of ABZ was maintained as observed by DSC and XRD analysis. The NC approach was able to improve the dissolution percentage of ABZ by approximately three-fold. Furthermore, the incorporation of NCs into DMNs using the combination of poly(vinylpyrrolidone) and poly(vinyl alcohol) formed sharp needles with sufficient mechanical strength and insertion properties. Dermatokinetic studies revealed that >25% of ABZ was localized in the dermis of excised neonatal porcine skin up to 48 h after DMN administration. In *in vivo* pharmacokinetic studies, the AUC and relative bioavailability values of ABZ delivered by NC-loaded DMNs were found to be significantly higher than those obtained after oral administration of coarse suspension of ABZ or ABZ-NCs, as well as DMNs delivering coarse ABZ as indicated by the relative bioavailability values of >100%. Therefore, the combination approach developed in this study could maintain the systemic circulation of ABZ, which could be possibly caused by avoiding the first-pass metabolism in the liver. This could be beneficial to improve the efficacy of ABZ in CE treatment.

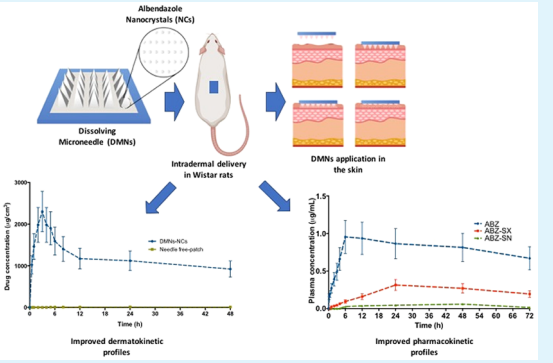

KEYWORDS: *Albendazole, nanocrystals, microneedles, cystic echinococcosis, pharmacokinetics*

Downloaded via UNIV OF GLASGOW on August 11, 2021 at 18:25:46 (UTC).
See https://pubs.acs.org/sharingguidelines for options on how to legitimately share published articles.

1. INTRODUCTION

Cystic echinococcosis (CE) is a devastating zoonosis which affects both humans and animals. CE is caused by *Echinococcus* spp., commonly *Echinococcus granulosus*.[1,2] After infecting a human, *Echinococcus granulosus* enters the systemic circulation and is accumulated in the liver and other organs, forming hydatid cysts.[3] This infectious disease causes a significant public health issue worldwide, including areas of central South America, Asia, and even in Mediterranean countries.[4] Moreover, although the infected body produces humoral immune and specific cellular responses, a persistent cohabitation of *Echinococcus granulosus* and has been found to be the main challenge in this disease.[5,6] Additionally, CE has been considered as a neglected tropical disease (NTD) by The World Health Organization (WHO), and it has been estimated that around 1−3 million disability cases have been reported as a result of this disease per annum.[7] Furthermore, around US $3 billion have been spent yearly because of direct and indirect effects of this disease on both humans and livestock.[8]

Presently, there are several choices for the treatment of CE. These include antiparasitic administration, surgical intervention, and percutaneous drainage therapy. The selection of treatments is dependent on the nature of the cysts in each patient.[9] The administration of antiparasitic agents is the first treatment option where doctors are not available. Additionally, this is the only alternative in numerous inoperable circumstances, including cysts in the brain and cysts in patients who

Received: June 15, 2021
Accepted: July 26, 2021

© XXXX American Chemical Society

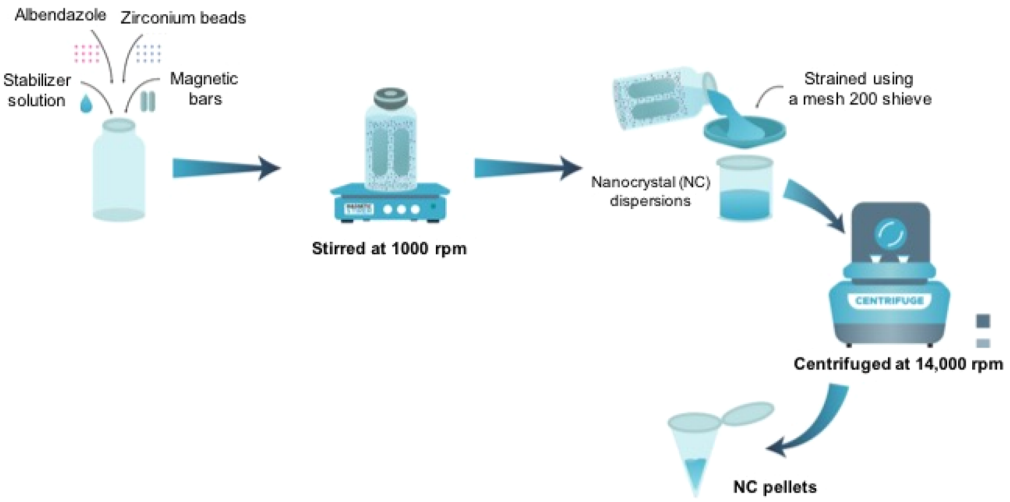

Figure 1. Schematic representation of NC preparation.

are immune-suppressed.[10] Currently, the benzimidazole carbamate derivate, albendazole (ABZ), is the most effective drug commonly used for the treatment of CE. However, ABZ has poor aqueous solubility, resulting in low bioavailability when administered orally. This leads to lack efficacy with only one-third of patients suffering from hydatid cysts showing complete remission and 20−40% of patients not responding to ABZ therapy.[11] Consequently, the drug should be taken in high doses (10−15 mg/kg of body weight) and for long periods (3−6 months), leading to liver toxicity, gastrointestinal toxicity, and other side effects.[12−14] In addition, due to its low solubility in aqueous environments, the route of administration options are limited to the oral route.[15,16] Therefore, it is crucial to develop a formulation which can overcome the poor solubility.

Multiple approaches have been explored in order to improve the biopharmaceutical performance of ABZ, including the formulation of solid dispersions,[17] oil-in-water emulsions,[18] inclusion complexes with cyclodextrins,[19] cogrinding with hydrophilic excipients,[20] liposomes,[21] nanocapsules,[22] chitosan microspheres,[23] and nanocrystals (NCs).[24−26] Although these efforts have been partially successful in increasing the dissolution rate and *in vivo* absorption of the drug, they were developed for oral administration. When administered orally, ABZ encounters rapid first-pass metabolism in the liver, being transformed into ABZ-sulfoxide (ABZ-SX).[27] Although ABZ and ABZ-SX show antiparasitic activities, ABZ has been reported to possess stronger affinity to parasite tubulins when compared to ABZ-SX, meaning that ABZ has higher activity than ABZ-SX.[28] It has also been reported that the viability of cysts in NMRI mice infected by *Echinococcus granulosus* was lower after the administration of ABZ compared to those with the administration of ABZ-SX.[29] Accordingly, a new delivery approach which can avoid the rapid metabolism of ABZ in the liver may enhance the efficacy of ABZ in the treatment of CE.

Transdermal delivery systems are one of the most favorable methods to improve the delivery of numerous drugs and are able to avoid hepatic first-pass metabolism,[27,30] Among various delivery approaches, dissolving microneedles (DMNs) have shown numerous advantages compared to other strategies,[31] since they bypass the skin's *stratum corneum*.[32] DMNs are composed of needles <1 mm in height. Importantly, the application in human volunteers did not result in any pain, providing compliant administration.[33] Furthermore, postapplication, DMNs administration does not produce any biohazardous waste.[27,34]

Among the strategies used to enhance the dissolution rate of the poorly soluble drugs mentioned above, the formulation of nanocrystals (NCs) is one the most attractive and has been widely used due to its flexibility, scalability, and high drug loading efficiency.[35] This approach has resulted in more than 20 approved products in the market globally.[36] NCs are described as nanometer-sized drug particles without matrix substances in crystalline form, consisting of up to 90% hydrophobic drugs which are generally stabilized by surfactants.[37] NCs enhance the saturation solubility and the rate of dissolution of hydrophobic drugs by reducing the particle size and thus enlarging their surface area.[38] This approach has been successfully applied in the formulation of several hydrophobic drugs, including curcumin,[39] budesonide,[40] and a number of highly hydrophobic antifungal drugs,[41−43] displaying that the dissolution rates of the aforementioned drugs were significantly improved. Importantly, the combination of NCs and DMNs technologies has shown promising results in the systemic delivery of poorly soluble drugs for both local and systemic effects.[44] Considering the significant advantages of DMNs and NCs, the delivery approach combining these systems could be a favorable choice to maintain the systemic availability of ABZ for improved effective therapy of CE.

In the present study, we develop, for the first time, the combinatorial approach of NCs and DMNs for the intradermal administration of ABZ using to improve its bioavailability. Initially, the NCs were developed using the top-down method and using an ultrasmall-scale media mill. Several characterizations were further performed, including particle size, polydispersity index, physical characteristics, and drug release kinetics and were further characterized. Subsequently, the NCs were loaded into DMNs and characterizations of mechanical properties were carried out. Moreover, *ex vivo* dermatokinetic studies were also performed to examine the intradermal delivery of this approach. Finally, *in vivo* pharmacokinetic studies of ABZ in NCs after DMN administration in rats were compared to the conventional administration of ABZ in CE therapy.

https://doi.org/10.1021/acsami.1c11179
ACS Appl. Mater. Interfaces XXXX, XXX, XXX−XXX

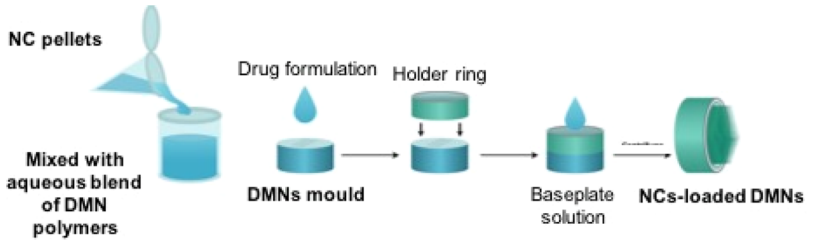

Figure 2. Schematic representation of two-layered DMN preparation.

2. EXPERIMENTAL SECTION

2.1. Materials. Albendazole and albendazole sulfone (purity, ≥98%) of analytical grade were purchased from Alfa Aesar (Lancashire, U.K.). Albendazole sulfoxide (purity, ≥98%), polyoxyethylene (20) sorbitan monooleate (Tween80), and poly(vinyl alcohol) (PVA) (9−10 kDa) and PVA (31−50 kDa) were obtained from Sigma-Aldrich (Dorset, U.K.). Poly(vinylpyrrolidone) PVP (58 kDa) was obtained from Ashland (Kidderminster, U.K.). Pluronic F127 (P127) was gifted by BASF SE (Ludwigshafen, Germany). Yttria-stabilized zirconia beads of 0.5 mm diameter were obtained from Chemco Advance Material (Suzhou, China). Importantly, other reagents were all obtained from standard commercial suppliers and were analytical grade.

2.2. Fabrication of ABZ-NCs. A media milling technique utilizing an ultrasmall-system assembly was applied to prepare ABZ-NCs,[45] with minor changes. The system consisted of small glass vial with volume of 12 mL, two magnetic bars of (12 × 8 mm) and magnetic stirrer, as shown in Figure 1. Initially, 0.25 g of ABZ, 8 g of zirconia beads, and 10 mL of stabilizer were put in the glass vial. Afterward, two magnetic bars were added into the system. Then, the system was locked with an airtight cap. The formulation was stirred for 24 h at 1000 rpm on magnetic stirrer (IKA, Staufen, Germany). In order to obtain the optimum time process, samples were taken at predetermined interval times for particle size determinations. Subsequently, to separate the zirconia beads and the magnetic bars, the dispersion obtained was strained using a mesh 200 sieve. In this study, Tween 80, P127, or PVA with the concentrations of 0.5% w/v, 1% w/v, and 2% w/v in water were screened as a stabilizer.

2.3. Characterization of ABZ-NCs. Dynamic light scattering (DLS) utilizing a particle size analyzer (NanoBrook Omni, Brookhaven, New York, U.S.A.) was applied in order to determine particle size and polydispersity index of ABZ-NCs. The measurements were done in triplicate. To observe the morphology of ABZ-NCs, scanning electron microscopy (SEM) (TM3030 microscope, Hitachi, Krefeld, Germany) was used. The coarse dispersion of ABZ in water was also observed as comparison.

In order to investigate the chemical interactions of each component in the formulation, a Fourier transform infrared (FTIR) spectrometer (Accutrac FT/IR-4100 Series, PerkinElmer, U.S.A.) was used. Additionally, the crystallinity of ABZ-NCs was observed using two different methods, namely differential scanning calorimetry evaluation (DSC 2920, TA Instruments, Surrey, U.K.) and an X-ray diffraction analysis (Rigaku Corporation, Kent, England). Coarse ABZ powder, ABZ-NCs and physical mixture (PM) of the optimized formulation were used for these studies.

2.4. Investigation of *In Vitro* Release. A dialysis method was used to assess the *in vitro* release of ABZ-NCs in comparison with coarse ABZ.[46] The release study was carried out in PBS (pH 7.4) containing 1% w/v of Tween 80. Briefly, ABZ (10 mg) and ABZ-NCs (containing 10 mg of ABZ) were placed into dialysis membrane. Membrane used in this study possessed 12 000−14 000 molecular weight cutoff (MWCO) (Spectra-Por, Spectrum Medical Industries, Los Angeles, CA, U.S.A.). Initially, the membrane was then placed into 100 mL of dissolution media. The study was performed for 24 h and at 37°C at 100 rpm. At predetermined times, 1 mL of release medium was taken and replaced with 1 mL of fresh medium. Finally, the amount of ABZ released was analyzed using HPLC. The drug release percentages were then calculated using eq 1

$$\text{The drug release percentage} = \frac{\text{ABZ detected in the release study}}{\text{initial amount of ABZ}} \times 100 \quad (1)$$

The drug release profile of ABZ from ABZ-NCs was fitted to various mathematic models, namely zero order, first order, Higuchi, Korsmeyer-Peppas, and Hixson-Crowell.[33,41] DDsolver (China Pharmaceutical University, Nanjing, China) was used to determine the parameters of each model.

2.5. Fabrication of Two-Layered DMNs. In order to incorporate the NCs into DMNs, initially the NCs obtained were centrifuged for 30 min at 14 000 rpm using a centrifugation system (Sigma 1-14 microcentrifuge, SciQuip Ltd., Shropshire, U.K.). This step was repeated three times in order to wash the NCs using distilled water, generating washed NCs pellets. The DMNs matrix used was an aqueous blend of the mixture of 25% w/w of PVP (58 kDa) and 15% w/w of PVA (31−50 kDa). As template, silicone molds were employed to fabricate the two-layered DMNs. The molds were prepared utilizing the transparent LSR9-9508-30 silicone elastomer mix (part A/part B 1:1 w/w). The molds possessed 16 × 16 needles with pyramidal shapes. The height of each needle was 850 μm with 250 μm base colum and 600 μm pyramidal tip. The base and interspacing between each needle were 300 μm.[47] To develop the DMN formulation, the first layer of DMNs containing ABZ-NCs and DMNs matrix was prepared in five different NC concentrations, namely 10% ABZ-NCs (Formulation A), 20% ABZ-NCs (Formulation B), 30% ABZ-NCs (Formulation C), and 40% ABZ-NCs (Formulation D). The second layer of the formulation was the polymeric solution containing PVP (90 kDa) 30% w/w. To enhance the elasticity, the second layer solution was mixed with glycerol 1.5% w/w. Figure 2 shows the schematic representation of two-layered DMN preparation. Following the mixing process, casting process of the first layer was conducted by pouring the formulation onto the DMN molds. Afterward, the molds were put in a positive pressure chamber for 2 min and pressure of 5 bar was applied. Then, the excess formulation was removed from the top of the molds. To facilitate the attachment of the second layer, a silicone ring was fixed to the MN molds.[48,49] Then, the second layer formulation (850 μL) was poured on top of the first layer, secured by the holder ring. The molds were then centrifuged for 15 min at 3500 rpm. The drying process was divided into two steps. For the first 24 h, the formulations were dried at room temperature. Finally, the formulations were dried at 37°C for 12 h.

2.6. Morphology Observation of Two-Layered DMNs. The morphologies of DMNs containing ABZ-NCs were visualized. Two different methods were used, namely, light microscopy using A Leica EZ4D light microscope (Leica Microscope, Milton Keynes, U.K.) and scanning electron microscopy using SEM TM3030 (Hitachi, Krefeld, Germany).

2.7. Assessment of Mechanical and Insertion Properties of Two-Layered DMNs. The mechanical strength of DMNs laden with ABZ-NCs was examined using a TA.XT2 Texture Analyzer (Stable Micro Systems, Haslemere, U.K.), as reported previously. The force applied was 32 N/array for 30 s.[50] The mechanical strength was presented by the height percentage reduction of DMNs after the compression compared to the height before the compression.

https://doi.org/10.1021/acsami.1c11179
ACS Appl. Mater. Interfaces XXXX, XXX, XXX−XXX

The insertion ability of DMNs in both full-thickness neonatal porcine skin and an established skin-simulant artificial membrane, ParafilmM was examined utilizing an optical coherence tomography (OCT) microscope (Michelson Diagnostics Ltd., Kent, U.K.), as published earlier.[32,50,51] The study was carried out by inserting the DMNs using a texture analyzer with the force of 32 N/array for 30 s into eight layers of ParafilmM. The number of holes created in each layer of ParafilmM following the insertion of DMNs was counted. Furthermore, the visualizations of DMNs insertion and penetration depth into full-thickness neonatal porcine skin and ParafilmM were carried out using ImageJ (National Institute of Health, Bethesda, MD, U.S.A.).

2.8. Quantification of Drug Content Localized in the Needle Tips of DMN. To determine the quantity of ABZ in the needle tips of DMN, initially a scalpel was used to carefully detache the first layer of DMNs. The collected part was further solubilized in 10 mL of methanol. In order to completely dissolve ABZ, the mixture was placed for 1 h in a bath sonicator and centrifuged at 14 000 rpm for 15 min. The amount of ABZ in the supernatant was analyzed using HPLC.

2.9. Determination of Particle Size of ABZ-NCs in DMN Formulations. To evaluate the effect of DMN formulations on the size of ABZ-NCs, initially, the DMNs laden with ABZ-NCs were completely dispersed in distilled water. Following this step, the particle size and PDI of NCs and were determined using the similar technique and those values were equated to the initial particle size and PDI.

2.10. Microneedles Dissolution Study. The *in situ* skin dissolution time of DMNs was studied as per a method reported previously.[33] Briefly, the DMNs were inserted into the center of the skin section using manual pressure. A cylindrical stainless-steel weight (5.0 g) was positioned on top of the DMNs during the dissolution study. At defined time points, DMNs were detached from the skin, and the shape of DMNs was viewed utilizing the light microscope.

2.11. *Ex Vivo* Dermatokinetic Assessments. Evaluation of *ex vivo* dermatokinetic of ABZ from DMNs-NCs formulation were conducted in excised full-thickness porcine skin in Franz cell diffusion cells using a technique described in our previous publications.[27,32] Initially, the DMNs were inserted manually into the skin and the skin was fixed into Franz cell diffusions using cyanoacrylate glue. In this study, PBS (pH 7.4) and 1% w/v of Tween 80 were used as receptor medium. The cylindrical stainless-steel weight (5 g) was put on top of the DMNs. The experiment was carried out at 600 rpm at 37 ± 1 °C. The skin samples were taken at defined interval times, separated from DMNs, and washed with PBS. Then, the skin was pierced using a biopsy punch with diameter of 5 mm (Stiefel, Middlesex, UK). To separate the epidermis from the dermis layers, the skin samples were heated in a water bath for 2−3 min at 60 °C. The epidermis was carefully separated from the dermis using forceps. Following this step, ABZ was extracted from the skin by adding 1 mL of methanol to the skin sections and the mixture was then homogenized using Tissue Lyser LT (Qiagen, Ltd., Manchester, U.K.) at 50 Hz for 10 min. The determination of ABZ was carried out using HPLC. A curve comprising the drug concentration versus time of application was made and PKSolver (China Pharmaceutical University, Nanjing, China)[52] was applied to calculate the dermatokinetic profiles using a one-compartment open model. The maximum drug concentration (C_{max}), the time of maximum concentration (t_{max}), the area under the curve from time zero ($t = 0$) to the last experimental time point ($t =$ 24 h) (AUC), the mean half-life ($t_{1/2}$) and the mean residence time (MRT) were all calculated. The dermatokinetic assessments of needle-free patches loaded with ABZ NCs (ABZ-NCs) were also carried out as a control.

The distribution and deposition study of ABZ in different skin depths were further evaluated. Briefly, skin samples after the administration of DMNs in different time points, namely 1 h, dermis t_{max} from the dermatokinetic study and 24 h were detached from Franz cell diffusion cells. Following this step, a silicone mold was filled with the skin samples, mixed with optimal cutting temperature (OCT) media media (Tissue TEK) and frozen using liquid nitrogen. Afterward, the sectioned skin samples with thickness of 50 μm were obtained using a Leica CM1900 Cryostat (Leica Microsystems, Nussloch, Germany). Afterward, this step was carried out until all of samples were completely cut. Five consecutive skin samples (total thickness of approximately 2.5 mm) were collected into the same microtube. Subsequently, ABZ was extracted from skin samples in 1 mL methanol, vortexed for 15 min, and centrifuged at 14 000×*g* for 15 min. Finally, the supernatant was taken and analyzed using HPLC.

2.12. *In Vivo* Study. *2.12.1. Assessment of the Pharmacokinetics of ABZ, ABZ-SX, and ABZ-SN in Wistar Rat's Plasma.* The *in vivo* pharmacokinetic assessment was carried out to evaluate the delivery of ABZ from DMNs-NCs in healthy male Wistar rats weighing 208.17 ± 13.31 g. This study was conducted in compliance with the Health Ethical Committee at the Faculty of Medicine, Hasanuddin University, Indonesia. One week before the *in vivo* experiment, the rats were adapted to the laboratory conditions. During the adaptation and the experiment periods, food and water were given *ad libitum*. The animals were divided into four cohorts (n = 5 per cohort) and treated as follows: Group A received 2× DMNs containing ABZ-NCs; Group B received 2× DMNs containing coarse ABZ; Group C received 1 mL of ABZ-NCs orally and Group D received 1 mL of ABZ coarse suspension. All cohorts received a dose which was equal to 15 mg/kg of ABZ.

For the groups receiving DMNs, the rats' hair on the back region was shaved using an electric clipper, followed by the use of hair removal cream (Veet). DMNs were initially attached to Microfoam tape and administered using finger pressure for 30 s onto the shaved area of the rats. Following this step, the DMNs were secured using Tegaderm (3 M, St Paul, Minnesota, U.S.A.). Then, Micropore tape (3 M U.K. Plc, Bracknell, Berkshire, U.K.) was applied on top of Tegaderm. Blood samples of the rats from all cohorts were taken at 0.5, 1, 2, 4, 6, 12, 24, 48, and 72 h. The blood collected was placed into an Eppendorf tube containing 3.8% w/v of sodium citrate. To obtain the plasma samples, tubes were centrifuged for 10 min at 4 °C at 3000×*g*. Prior to analysis, the plasma samples were kept at −20 °C.

2.12.2. Sample Preparation and Analyte Extraction. To extract ABZ from plasma samples after the *in vivo* pharmacokinetic studies, a simple one-step protein precipitation technique utilizing methanol was applied. First, in an Eppendorf tube, 500 μL of methanol was added to 100 μL of plasma. The mixture was vortexed for 10 min and centrifuged at 14 000×*g* at 4 °C for 15 min. The supernatant was collected and dried in a fume hood for 3 h in a glass vial. Afterward, 100 μL of the mobile phase was added into the residue. The mixture then was vortexed for 10 min. The supernatant was obtained by centrifugation at 14 000×*g* for 15 min. The samples were analyzed using HPLC. In addition to ABZ, ABZ-SX and ABZ-SN as the metabolites of ABZ, were also analyzed.

2.12.3. Calculation of Pharmacokinetic Parameters. The of drug concentration in plasma versus sampling time was constructed. The pharmacokinetic profiles were analyzed using a noncompartmental model. The maximum drug concentration (C_{max}), the time of maximum concentration (t_{max}), the area under curve from time zero ($t = 0$) to the last experimental time point ($t = 24$ h) (AUC), the mean half-life ($t_{1/2}$), and the mean residence time (MRT) were calculated using PK Solver.[52]

The relative plasma bioavailability (F) of ABZ following intradermal administration of NCs delivered from DMNs in comparison with oral administration was estimated using eq 2

$$F = \frac{\mathrm{AUC_{MN}} \times \mathrm{dose_{oral}}}{\mathrm{AUC_{oral}} \times \mathrm{dose_{MN}}} \times 100 \quad (2)$$

where $\mathrm{AUC_{MN}}$ is the AUC of plasma from DMNs administration and $\mathrm{AUC_{oral}}$ is the AUC of plasma oral administration of ABZ.

2.13. The Chromatographic Condition for ABZ Analysis. Quantification of ABZ in *in vitro* studies was performed using HPLC (Agilent Technologies 1220 Infinity U.K. Ltd., Stockport, U.K.). The stationary phase used in this study was Phenomenex Luna C_{18} (ODS1) column with internal diameter of 150 mm × 4.6 mm and particle size of 5 μm. The mobile phase used was the mixture of 25

https://doi.org/10.1021/acsami.1c11179
ACS Appl. Mater. Interfaces XXXX, XXX, XXX−XXX

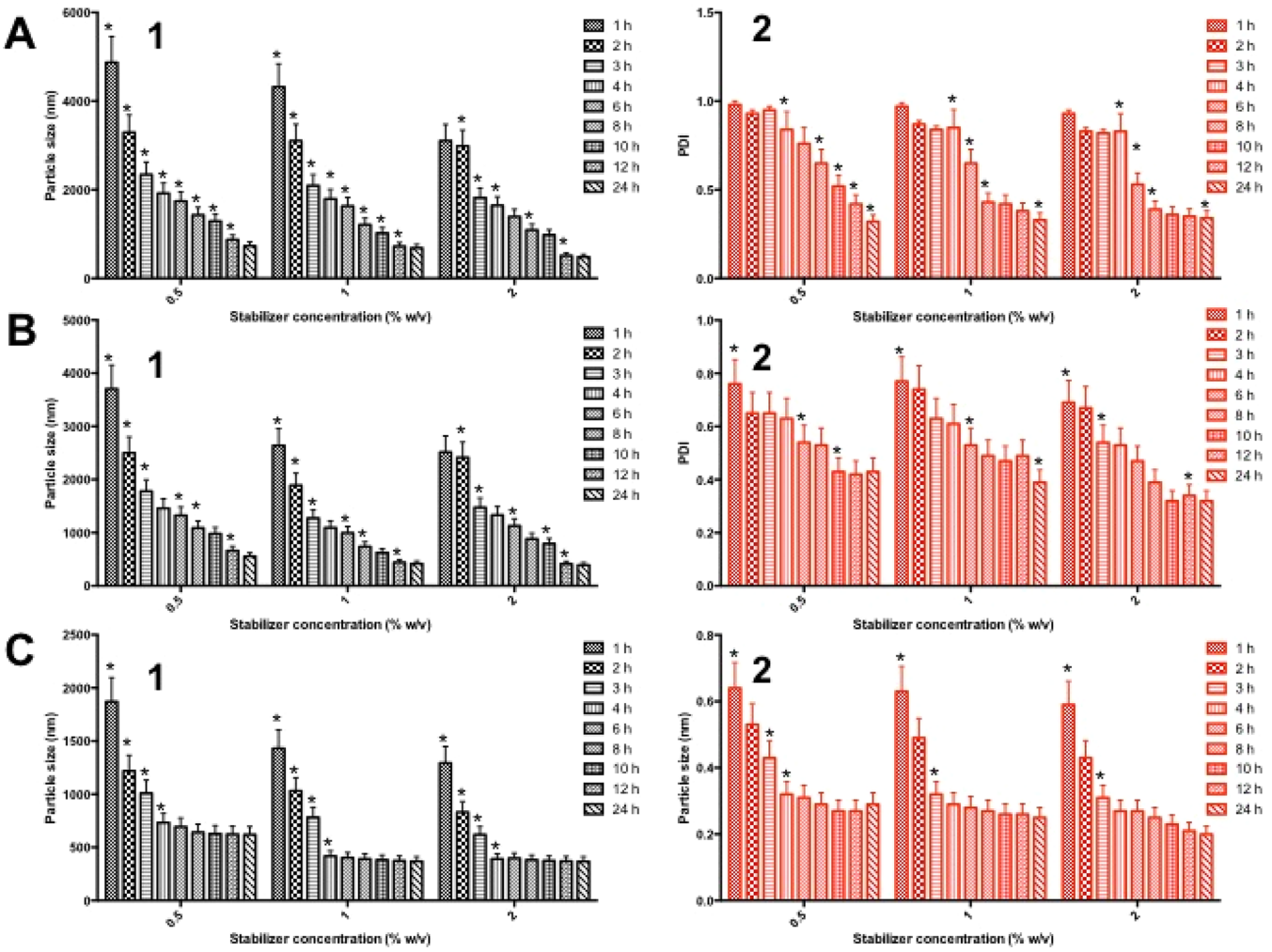

Figure 3. Particle size (1) and PDI (2) values of ABZ-NCs formulated using Tween 80 (A), PVA (B), and P127 (C) at 0.5, 1, and 2% w/v (mean ± SD, $n = 3$, * $p < 0.05$)

mM sodium dihydrogen phosphate buffer containing 0.1% v/v triethylamine (TEA) (pH 3) and methanol with a ratio of 75:25 v/v. The chromatographic conditions were flow rate of 1 mL/min and injection volume of 25 μL. The analyses were carried out at room temperature and all samples were detected at 290 nm. The analytical method was validated according to the International Conference on Harmonization (ICH) 2005. The limit of detection (LoD) and the limit of quantification (LoQ) values of ABZ were 0.002 μg/mL and 0.03 μg/mL, respectively.

In *in vivo* experiments, the analyses of ABZ, ABZ-SX, and ABZ-SN were carried out using HPLC (Shimadzu Prominence, Shimadzu, Kyoto, Japan). The analyses were conducted utilizing an Xselect CSH C18 column with 3.0 × 150 mm internal diameter and 3.5 μm particle size. The mobile phase used was the mixture of 0.1% v/v of trifluoracetic acid in water and methanol with a ratio of 75:25 v/v. The chromatographic conditions were flow rate of 1 mL/min, UV detection at 290 nm, and injection volume of 25 μL. The analyses were again carried out at room temperature. The bioanalytical assay was validated according to the International Conference on Harmonization (ICH) 2005. The LoD values were 0.003, 0.002, and 0.003 μg/mL, and theLoQ values were 0.02, 0.01, and 0.02 μg/mL for ABZ, ABZ-SX, and ABZ-SN, respectively.

2.14. Statistical Analysis. Statistical analysis was carried out using GraphPad Prism version 6 (GraphPad Software, San Diego, California, U.S.A.). All results were presented as mean ± standard deviation (SD). An unpaired t test was applied to analyze the results from two cohorts. To compare more than two cohorts, one-way ANOVA was applied. Data was considered significantly different when p values < 0.05.

3. RESULTS AND DISCUSSION

3.1. Fabrication and Characterizations of ABZ-NCs. In the present work, NCs-based formulations were developed to overcome the poor aqueous solubility of ABZ. Specifically, the top down technique using modified media milling was selected. This method forms NCs according to mechanical abrasion to transform large crystalline particles into nanosized particles.[53] Compared to the bottom up technique, this method has been reported to be more likely to maintain the crystalline form of the particles.[54] Several stabilizers were screened, including Tween 80, PVA, and P127, with different concentrations. The graphs presenting the particle size and PDI values in the screening proses are depicted in Figure 3.

Tween 80 produced particles possessing sizes in nanometer scales at the stabilizer concentrations of 0.5% w/v and 1% w/v after 12 h. Meanwhile, after 10 h the NCs were formed when 2% w/v of stabilizer was used. The particle sizes of NCs were found to be 732 ± 87 nm for 0.5% w/v, 683 ± 76 nm for 1% w/v, and 489 ± 38 nm for 2% w/v after 24 h. The PDI values obtained were more than 0.3, showing the wide distribution of the NCs. This could potentially result in physical instability of NCs due to the Ostwald ripening phenomenon.[55] Never-

https://doi.org/10.1021/acsami.1c11179
ACS Appl. Mater. Interfaces XXXX, XXX, XXX−XXX

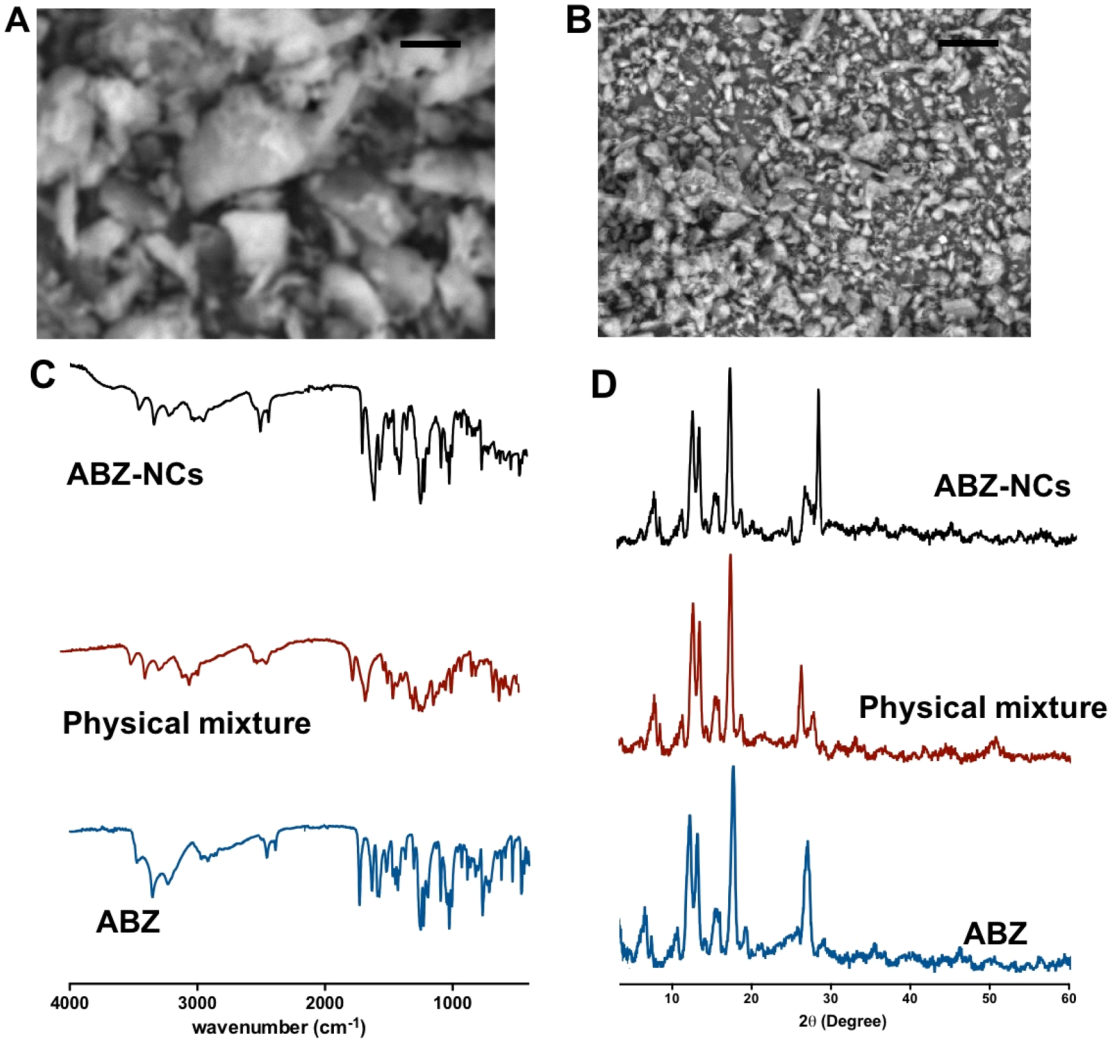

Figure 4. SEM images of coarse ABZ (A) and ABZ-NCs (B) at a magnification power of 30 000× (the black scale bar shows a length of 1 μm). FTIR spectra of ABZ, physical mixture and ABZ-NCs (C). X-ray diffractogram of ABZ, physical mixture, and ABZ-NCs (D).

theless, this phenomenon could only occur in the liquid environment. This can be circumvented by the removal of the solvent and changing the NCs dispersion into a solid state.[56] Accordingly, because DMNs are solid in their forms, the combination of NCs and DMNs could be potentially beneficial to avoid this instability. Moreover, the utilization of PVA as stabilizer could generate NCs after 10 h milling time for the concentration of 0.5% w/v and 8 h milling time for the concentrations of 1% w/v and 2% w/v. The PDI values were found to be more than 0.3. Specifically, the particle sizes obtained after 24 h were observed to be 626 ± 65 nm for 0.5% w/v the stabilizer concentrations, 372 ± 32 nm 1% w/v the stabilizer concentrations, and 368 ± 29 nm 2% w/v the stabilizer concentrations. The smallest particle sizes were obtained in the use of P127 as stabilizer. The NCs were formed after shorter milling time, 4 h for the stabilizer concentration of 0.5% w/v; 3 h for the stabilizer concentrations of 1% w/v and 2% w/v. After 24 h, the particle sizes of NCs were observed to be 621 ± 74, 369 ± 45, and 356 ± 39 nm for the concentrations of 0.5% w/v, 1% w/v, and 2% w/v, respectively. Importantly, the PDI values obtained were below 0.3, indicating narrow particle distributions.[24] The NCs stabilization prepared from P127 can be explained by the presence of hydrophobic poly(propylene oxide) (PPO) and hydrophilic poly(ethylene oxide) (PEO) chains.[32] The PPO chains of poloxamer facilitate the stabilizer to adsorb onto the hydrophobic surface of the drug crystals.[57] Furthermore, aggregation is inhibited by the extension of PEO chains into the aqueous phase, offering steric stabilization.[58] In this study, we found that, in comparison with the particle sizes with milling times of 4 h, the particle sizes after longer milling times, including 24 h did not considerably change ($p > 0.05$). Additionally, the particle sizes obtained by the use of 1% w/v P127 were not statistically different in comparison with those obtained from 2% w/v P127. Accordingly, with the aim to minimize the production time and the use of stabilizer, the NCs prepared from P127 with a concentration of 1% w/v and 4 h milling processing time, possessing 418 ± 52 nm particle size and 0.29 ± 0.03 PDI, were chosen for further steps.

In the NCs characterizations, several methods were applied. First, the morphology of ABZ-NCs was observed using SEM. The SEM micrographs of ABZ-NCs and coarse ABZ are exhibited in Figure 4. It was observed that the size of ABZ-NCs in SEM analysis was found to be similar to the size obtained in DLS measurement, which was around 300 nm.

Furthermore, the interactions between ABZ and excipients were also evaluated. The FTIR spectra of ABZ, physical mixture of NC formulation, and ABZ-NCs are presented in

https://doi.org/10.1021/acsami.1c11179
ACS Appl. Mater. Interfaces XXXX, XXX, XXX−XXX

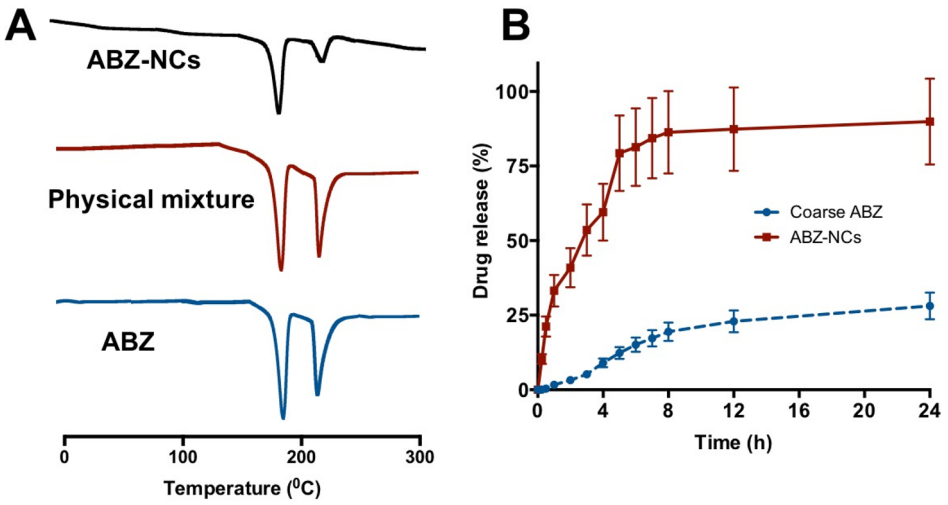

Figure 5. DSC thermogram of ABZ, physical mixture and ABZ-NCs (A). *In vitro* release percentages of ABZ from NC formulations compared to the coarse ABZ (mean ± SD, n = 3) (B).

Figure 4. The spectrum of FTIR of ABZ exhibited several absorptions, due to the presence of several functional groups. The signal identified at 1193 cm^{-1} could be due to the presence of the C—O—C bond. The signals observed at 1635 and 1572 cm^{-1} were attributed to the N−H out of the plane bending of ABZ structure. The presence of carbonyl groups was identified at 1709 cm^{-1}. In addition, the sharp peaks found at 2935 and 2878 cm^{-1} were due to the C−H stretching. Finally, the peaks at 3331 and 2705 cm^{-1} were detected, which might be due to the presence of N−H stretching and the hydrogen bond between imidazole-NH and carbamate carbonyl, respectively. Importantly, these peaks were also observed in the physical mixture and ABZ-NCs formulation. Therefore, it could be concluded that there was no formation of a new chemical bond between ABZ and excipient used in the NCs formulation. However, it is important to note that hydrophobic and van der Waals interactions cannot be observed by FTIR.

To further investigate the crystallinity of ABZ after NCs preparation, DSC and XRD analyses were then performed. The DSC thermogram of ABZ, physical mixture of NC formulation and ABZ-NCs are depicted in Figure 5. It was found that ABZ had a sharp endothermic peak representing the melting point of ABZ at 193 °C. Additionally, the melting point peak was followed by a recrystallization of the melt at 207 °C. These peaks were also observed in the physical mixture and ABZ-NCs formulation. The presence of the melting point peak indicated the crystal form of ABZ. The crystallinity was also observed in XRD examination, displaying sharp signals at 2θ values of 6.63, 11.73, 16.72, 19.82, and 27.92 in ABZ, physical mixture, and ABZ-NCs, respectively (Figure 4). Accordingly, the formulation of NCs using media milling allowed maintenance the crystallinity of ABZ.

3.2. Investigation of *In Vitro* Release. Following its formulation into NCs, the *in vitro* release of ABZ was compared to the release of pure ABZ, as shown in Figure 5. After 24 h, only 28.11 ± 4.32% cumulative release was achieved from pure ABZ. On the other hand, the ABZ NCs improved the *in vitro* release of ABZ, showing percentage release of 89.92 ± 11.02% (approximately three times higher than pure ABZ) after 24 h. After statistical analysis, it was found that the release percentage of ABZ from NCs after 24 h was significantly greater (p = 0.017) in comparison to ABZ without NC formulations. The increase in the percentage of cumulative release of ABZ following the NCs formulation is related to the expanded specific surface of ABZ after the particle size reduction, resulting in an enhancement in the dissolution rate.[24,59]

In an attempt to determine the release mechanism of ABZ from NCs formulation, the release profile was fitted to various kinetic models. The results revealed that the values of correlation coefficient were 0.43 for zero-order, 0.92 for first-order, 0.56 for Higuchi, 0.81 for Korsmeyer-Peppas, and 0.76 for Hixson-Crowell, respectively. As the selection of the most suitable release model was performed according to the highest correlation coefficient value, the first-order kinetic model was found to be the most appropriate release model. Accordingly, concentration dependent was considered as the release mechanism of ABZ from the NCs formulation.[32,60] Several studies have shown the suitability of this model in describing several NC formulations.[32,41,48]

3.3. Fabrication and Morphology Observation of Two-Layered DMNs. As previously discussed, the main aim of this study was to incorporate ABZ-NCs into DMNs. Here, an aqueous blend containing a specific combination of PVA and PVP was selected. These polymers have been extensively utilized as polymer matrixes for DMN formulations. On the basis of our previous investigation, the combination of PVA and PVA could produce DMNs with better characteristics when compared to DMNs prepared from PVA alone or PVP alone. This may be explained by the interaction of −OH groups of PVA and C═O groups of PVP, forming hydrogen bonds.[27] A two-layered DMNs approach was selected in this study. This system offers several advantages. It has been reported that the permeation of hydrophobic drugs from DMNs only occurred in the needle parts of DMNs. Therefore, to prevent drug waste in the baseplate of DMNs, the drug was only localized in the needles.[27,61] Moreover, our initial investigation showed that the DMNs containing ABZ-NCs in the whole DMNs exhibited poor mechanical properties. Therefore, it was crucial to formulate the DMN baseplates using a different formulation. In this case, an aqueous blend containing 1.5% w/w glycerol and 30% w/w PVP (360 kDa) was used as a second layer baseplate. In the first layer, several formulations were screened in order to achieve a formulation

https://doi.org/10.1021/acsami.1c11179
ACS Appl. Mater. Interfaces XXXX, XXX, XXX−XXX

with high drug loading and adequate mechanical properties. After preparation, all DMNs were observed by a light microscope and a SEM, as shown in Figure 6. All DMNs

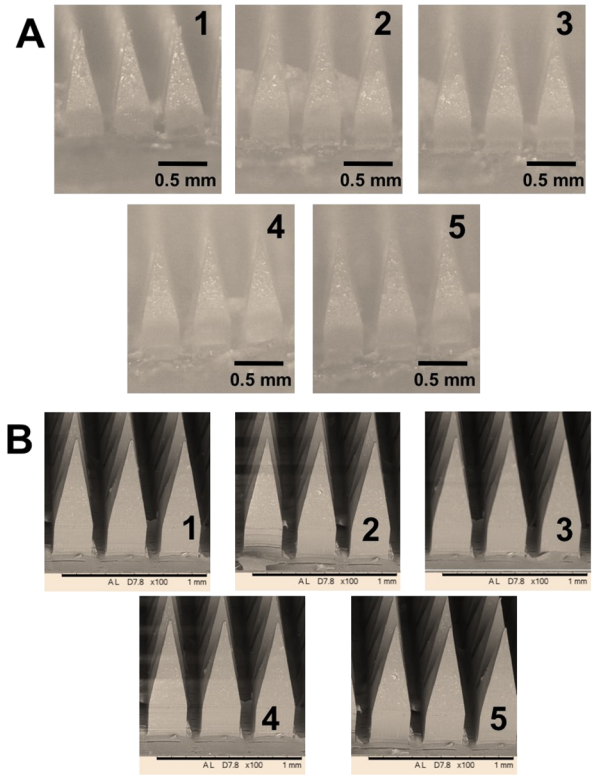

Figure 6. Light microscope pictures (A) of the DMN formulations prepared from 10% ABZ-NCs (Formulation A) (1), 20% ABZ-NCs (Formulation B) (2), 30% ABZ-NCs (Formulation C) (3), 40% ABZ-NCs (Formulation D) (4), and 50% ABZ-NCs (Formulation E) (5). SEM images (B) of the MN formulations containing 10% ABZ-NCs (Formulation A) (1), 20% ABZ-NCs (Formulation B) (2), 30% ABZ-NCs (Formulation C) (3), 40% ABZ-NCs (Formulation D) (4), and 50% ABZ-NCs (Formulation E) (5).

prepared in this study exhibited homogeneous polymer mixtures with sharp needle tips formed. Thus, all formulations were evaluated for their mechanical and insertion properties.

3.4. Assessment of Mechanical and Insertion Properties of Two-Layered DMNs. After the fabrication process, the DMNs containing ABZ-NCs were further characterized for their mechanical strength. This property is crucial because DMNs should have an adequate strength to penetrate the skin to deliver their drugs' cargo. The strength was evaluated based on needle height reduction percentage following compression with 32 N/DMN array.[62] The mechanical properties presented by the percentage of the height reduction of all DMN formulations are exhibited in Figure 7. The percentages of the height reduction were calculated to be 10.63 ± 2.81%, 11.65 ± 2.19%, 11.97 ± 3.02%, 12.87 ± 3.21%, and 19.76 ± 2.65% for Formulation A, Formulation B, Formulation C, Formulation D and Formulation E, respectively. The percentage needle height reductions between Formulation A, Formulation B, Formulation C, Formulation D, and Formulation E was not considerably different ($p > 0.05$). Nevertheless, the percentage needle height that decreased for the DMNs containing 50% w/w ABZ-NCs (Formulation E) was significantly ($p < 0.05$) higher compared to other formulations, indicating the decrease of mechanical strength of Formulation E. Accordingly, the mechanical properties of DMNs in this study were affected by the drug cargo concentration.

In addition to the mechanical strength, the insertion ability of DMNs was further evaluated. In this study, ParafilmM was employed as an established skin-simulant membrane. This artificial membrane has been established to replicate human skin in MN insertion assessment.[62] The results of this evaluation were depicted in Figure 7. Similar to the outcomes from the mechanical characteristics assessment, Formulation A, Formulation B, Formulation C, and Formulation D were able to penetrate four layers of ParafilmM. Considering that the thickness of each layer was approximately 126 μm, around 54% (504 μm insertion) of the needle tips of DMN of those formulations were inserted into the skin-stimulant membrane. In contrast, only two layers of ParafilmM were able to be penetrated by Formulation E, a percentage insertion of less than 50%. Accordingly, Formulation E developed in this study possesses the lowest mechanical and insertion abilities. Formulation D with the highest drug loading ability (40% w/w) was thus selected for further studies. The selected formulation was then characterized by visualizing visualization using OCT. This technique has been employed to study the insertion profiles of DMN in various studies.[50,63−67] The insertion visualizations were observed in the ParafilmM and the full-thickness neonatal porcine skin. Figure 7C,D represents the OCT micrographs illustrating the insertion of Formulation D into the ParafilmM and the full-thickness neonatal porcine skin. It was found that Formulation D was able to penetrate the ParafilmM and the full-thickness porcine skin until the depth of 501.59 ± 23.47 and 505.29 ± 19.82 μm, respectively. The results obtained in the OCT evaluation were found to be similar to the insertion investigation results observed in the percentages of holes produced in ParafilmM.

3.5. Quantification of Drug Content Localized to the Needle Tips of DMN. The quantity of drug localized in the needle tips of DMN was also the critical point in order to estimate the dose. Accordingly, after the drying process the amount of ABZ in the needle tips of DMN was further determined. It was found that the amount of ABZ localized in the needle tips of DMN was 3.79 ± 0.51 mg. Therefore, this amount was considered as the dose of ABZ in one DMN array in the further studies.

3.6. Determination of Particle Size of ABZ-NCs in DMN Formulations. The properties of NCs, particularly the particle size and PDI, after the incorporation into DMNs were evaluated. It is important to note that these properties should not be influenced by DMN preparations. The results showed that in DMN preparations, the properties of ABZ-NCs were observed to be 423 ± 43 nm and 0.26 ± 0.03 for the particle size and PDI, respectively. After statistical analysis, it was found that there were no significant differences ($p > 0.05$) in these properties in comparison with the initial properties.

3.7. Dissolution Study. The *ex vivo* skin dissolution evaluation was carried out to estimate the time needed by DMNs to dissolve completely following application to skin. DMNs containing ABZ-NCs were partially liquefied and showed a decrease in needle height after 10 min of application, as observed in Figure 8. The DMNs reached complete dissolution within 30 min of application to the skin.

3.8. *Ex Vivo* Dermatokinetic Studies. This study was designed to deliver the NCs into the dermis layer, where the drugs would be released for subsequent absorption into the

https://doi.org/10.1021/acsami.1c11179
ACS Appl. Mater. Interfaces XXXX, XXX, XXX−XXX

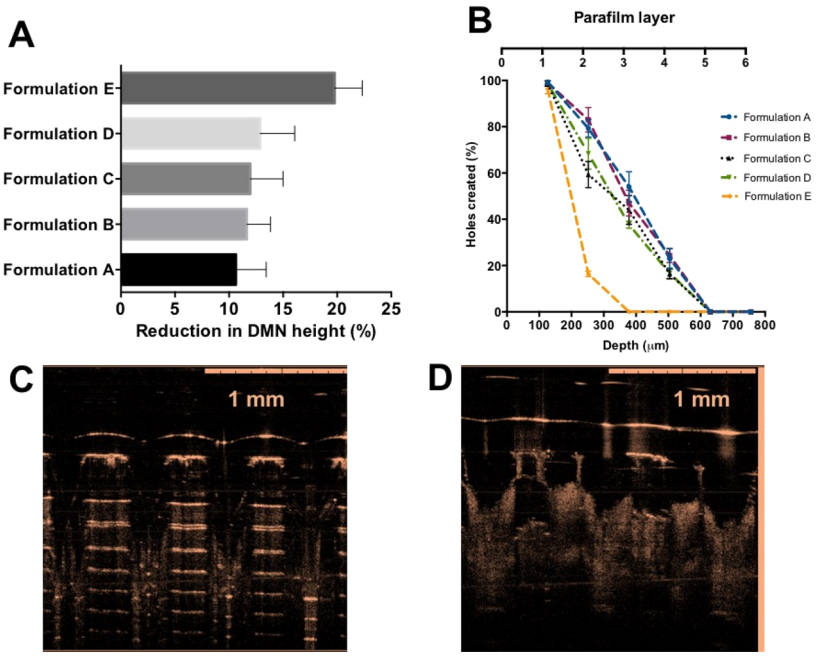

Figure 7. Percentage of height reduction of needles on the DMN arrays prepared from ABZ-NCs (mean ± SD, $n = 3$) (A). The percentage of holes generated in ParafilmM layers, applying an insertion force of 32 N/array for DMN formulations fabricated from ABZ-NCs (mean ± SD, $n = 3$) (B). Illustrative OCT micrographs of Formulation D following insertion into ParafilmM film (C) and full-thickness porcine skin (D).

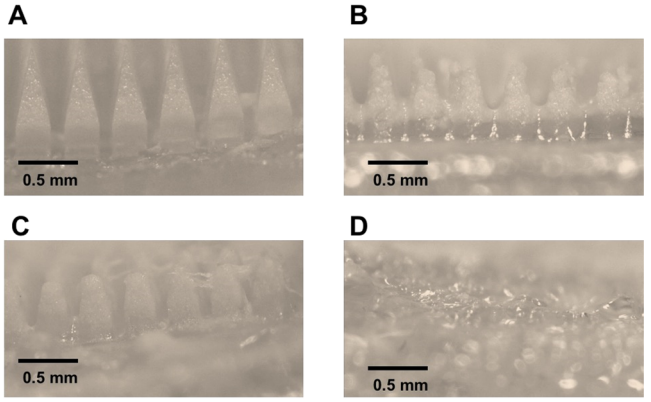

Figure 8. *Ex vivo* dissolution profiles of Formulation D at 0 min (A), 10 min (B), 20 min (C), and 30 min (D) observed using digital microscope after insertion into and removal from excised neonatal porcine skin.

systemic circulation by dermal capillaries. Thus, the release kinetics of ABZ from NCs after being delivered by DMNs into the skin were investigated using *ex vivo* dermatokinetic analysis. This method has been useful to evaluate the *ex vivo* skin kinetic profiles of numerous drugs delivered by DMNs.[27,32,33,68] Needle-free patches were used as a control and were also evaluated for their dermatokinetic profiles. It was discovered that the ABZ concentrations localized in the dermis and epidermis layer after the application of needle-free patches of ABZ were considerably lower ($p < 0.05$) in comparison with the ABZ concentration in the skin layers after the administration of DMNs. Therefore, this result revealed that DMNs could increase the intradermal delivery of ABZ.

Following the penetration of DMNs into the skin, the DMNs absorbs skin interstitial fluid. The polymers are then hydrated and fully dissolved. Afterward, the drug particles are released and diffuse into the deeper skin layers.[27] Figure 9 presents the comparison of ABZ concentration delivered in the epidermis and dermis after the administration of DMNs compared to the administration of a needle-free patch. Moreover, Table 1 presents the dermatokinetic parameters of ABZ following intradermal delivery using DMNs-NCs, namely C_{max}, T_{max}, $T_{1/2}$, AUC, and MRT. As shown, the C_{max} values of ABZ following DMNs application were observed to be 415.69 ± 64.31 $\mu g/cm^3$ at 2.07 ± 0.29 h and 1891.53 ± 273.83 $\mu g/cm^3$ at 2.79 ± 0.41 h in the epidermis and dermis, respectively. Furthermore, in the epidermis and the dermis, the AUC values were 10523.40 ± 2732.88 and 56615.29 ± 8919.79 $h \cdot \mu g/cm^3$, respectively. Following statistical analysis, the C_{max} and AUC value of ABZ in the dermis were significantly greater ($p < 0.05$ each) than the value in the epidermis. Importantly, the values of all parameters of dermatokinetic profiles of ABZ after the administration of needle-free patches were drastically lower ($p < 0.05$) in comparison with the obtained results after DMNs-NCs application.

In addition to the dermatokinetic profiles, the distributions of ABZ in various layers of full-thickness porcine skin were investigated. In this study, three time points, that is 1 h, t_{max} of dermatokinetic parameters, and 48 h after the administration of DMNs-NCs were chosen. It was found that ABZ was well-localized in various depths of the skin until a depth of 2.5 mm following the application of DMNs-NCs (Figure 10). This study showed that the longer application time was able to result in the increase of ABZ concentration in the lower areas on the skin, indicating the movement of ABZ-NCs in the skin.

Particularly, the maximum concentrations of ABZ were found to be 211.06 ± 47.19, 554.52 ± 121.13, and 107.91 ± 19.92 $\mu g/cm^3$ at depths of 0.9, 1.3, and 1.5 mm, respectively. On the other hand, with respect to needle-free patch distribution ABZ was only detectable until a depth of 1.1 mm. Additionally, the skin distribution of ABZ after the administration of a needle-free patch was found to be statistically lower ($p < 0.05$) compared to DMNs-NCs,

https://doi.org/10.1021/acsami.1c11179
ACS Appl. Mater. Interfaces XXXX, XXX, XXX−XXX

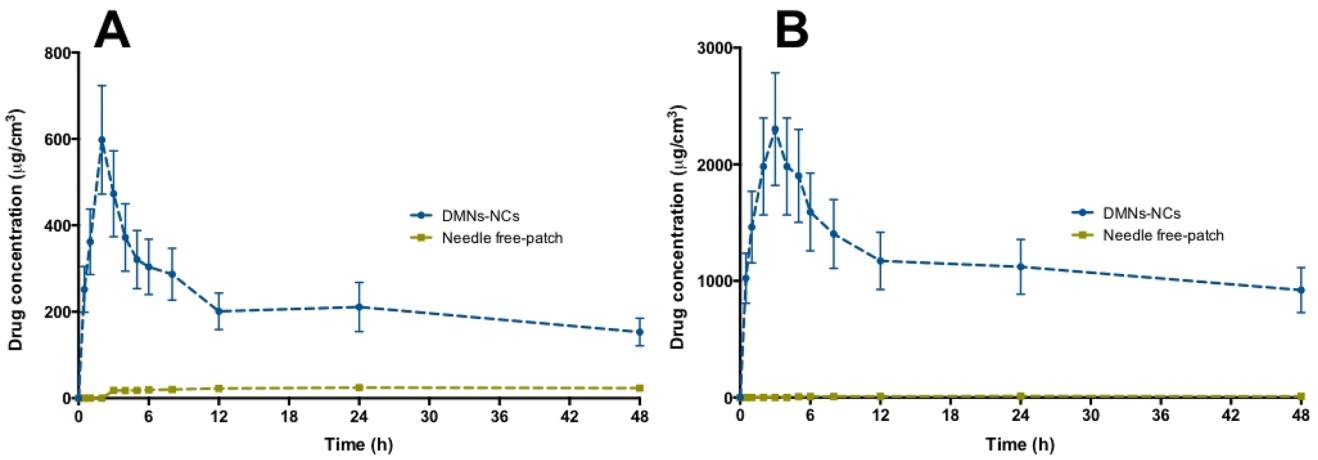

Figure 9. ABZ concentration and time profile in epidermis (A) and dermis (B) layers of excised full-thickness neonatal porcine skin, following the application of DMNs compared to needle-free patches laden with ABZ-NCs (mean ± S.D., n = 3).

Table 1. Parameter Dermatokinetic Profiles of ABZ in Epidermis and Dermis Layers of Excised Full-Thickness Neonatal Porcine Skin, Following the Application of DMNs Compared to Needle-Free Patches Laden with ABZ-NCs[a]

parameters	epidermis	dermis
C_{max} ($\mu g/cm^3$)	415.69 ± 64.31	1891.53 ± 273.83
T_{max} (h)	2.07 ± 0.29	2.79 ± 0.41
AUC (h·$\mu g/cm^3$)	10523.40 ± 2732.88	56615.29 ± 8919.79
$T_{1/2}$ (h)	20.44 ± 4.19	28.13 ± 5.63
MRT (h)	29.99 ± 6.31	41.26 ± 8.17

[a]Mean ± SD, n = 3.

demonstrating the poor skin distribution after their administrations. The findings obtained in this study exhibited the benefit of the combination of DMNs and NCs in enhancing the delivery of ABZ in the dermis layer, where the drugs are absorbed by blood.[69]

3.9. *In Vivo* Studies. As previously discussed, intradermal delivery was considered as the most suitable option to deliver ABZ because this route could potentially circumvent the first-pass metabolism in the liver, avoiding the metabolism of ABZ. In this experiment, the pharmacokinetic parameters of ABZ and its metabolites, ABZ-SX and ABZ-SN in plasma, were assessed following being delivered using DMNs-NCs approach. Importantly, we compared the pharmacokinetic profiles of all compounds with the oral administration of ABZ-NC as the conventional administration route of ABZ for CE. Additionally, the pharmacokinetic studies were also performed for DMNs and oral administration for coarse ABZ.

In the *in vivo* experiment, following 24 h, we removed the DMNs from the rats and it was observed that all DMNs were completely dissolved in the rats' skin. We did not observe any signs of irritation on the skin of all the rats. Table 2 and Table 3 present the plasma pharmacokinetic parameters of all analytes in Wistar rats following the intradermal administration of DMNs-ABZ NCs and DMNs-coarse ABZ, as well as the oral administration of ABZ-NCs and coarse ABZ. Concentrations of ABZ, ABZ-SX, and ABZ-SN in plasma after the DMNs and oral administration of ABZ-NCs and coarse ABZ are shown in Figure 11. Furthermore, the values of the pharmacokinetic parameters are depicted in Table 2 and Table 3.

With respect to the C_{max} values following oral dosing of coarse suspension, the analytes reached the maximum concentrations at the concentrations of 1.52 ± 0.43 μg/mL for ABZ, 1.38 ± 0.29 μg/mL for ABZ-SX, and 0.09 ± 0.01 μg/mL for ABZ-SN. The AUC_{0-72} values were 0.74 ± 0.12 for ABZ, 13.01 ± 2.23 for ABZ-SX, and 1.02 ± 0.23 ± h·μg/mL for ABZ-SN. Being formulated into NCs, following oral administration the maximum plasma concentrations of ABZ, ABZ-SX, and ABZ-SN were found to be 2.43 ± 0.41, 2.98 ± 0.51, and 0.12 ± 0.02 μg/mL, respectively. The AUC_{0-72} values were observed to be 10.84 ± 2.31 for ABZ, 31.72 ± 6.52 for ABZ-SX, and 2.07 ± 0.41 ± h·μg/mL for ABZ-SN. After DMNs administration of coarse ABZ, the maximum concentrations of 0.29 ± 0.06 μg/mL (AUC_{0-72} value of 12.09 ± 1.33 h·μg/mL), 0.08 ± 0.01 μg/mL (AUC_{0-72} value of 2.70 ± 0.43 h·μg/mL), and 0.06 ± 0.01 μg/mL (AUC_{0-72} value of 2.82 ± 0.66 h·μg/mL) were found for ABZ, ABZ-SX, and ABZ-SN, respectively. After ABZ-NCs administration delivered by DMNs, the C_{max} values were calculated to be 0.96 ± 0.32 μg/mL for ABZ, 0.32 ± 0.07 μg/mL for ABZ-SX, and 0.06 ± 0.01 μg/mL for ABZ-SN with AUC_{0-72} values of 57.59 ± 12.49, 16.51 ± 3.62, and 2.88 ± 0.61 h·μg/mL, respectively.

As the main purpose of this study was to improve the bioavailability of ABZ, we focused on the pharmacokinetic profiles of ABZ in detail. Analyzed statistically, it was found that the C_{max} of ABZ following oral administration of ABZ-NC and coarse ABZ were statistically greater ($p < 0.05$) in comparison with the C_{max} values after DMN administration. C_{max} is the maximum (or peak) concentration of drug achieved in a specified compartment.[70] Furthermore, the AUC value is a pharmacokinetic parameter utilized in diverse ways according to the background of experimental.[70] In this study, this parameter was used as an index of the total drug exposure integrated over time in the body. Accordingly, AUC values can also be used to determine the amount of drug absorbed or the effectiveness of physiological processes to eliminate the drugs.[70,71] The $t_{1/2}$ represents the time required for half of the initial dose of drug administered to be eliminated from the body.[71,72] The MRT refers to the whole persistence of the drugs in the body and is, hence, the mean time that the drugs reside in the body. In this study, it was found that the $t_{1/2}$ values of ABZ following the oral administration of coarse ABZ, the oral administration of ABZ-NCs, the DMN administration of coarse ABZ, and the DMN administration of ABZ-NCs were determined to be 0.88 ± 0.17, 3.54 ± 0.67, 43.52 ± 8.09, and 136.18 ± 21.28 h, respectively. Moreover, MRT values

https://doi.org/10.1021/acsami.1c11179
ACS Appl. Mater. Interfaces XXXX, XXX, XXX−XXX

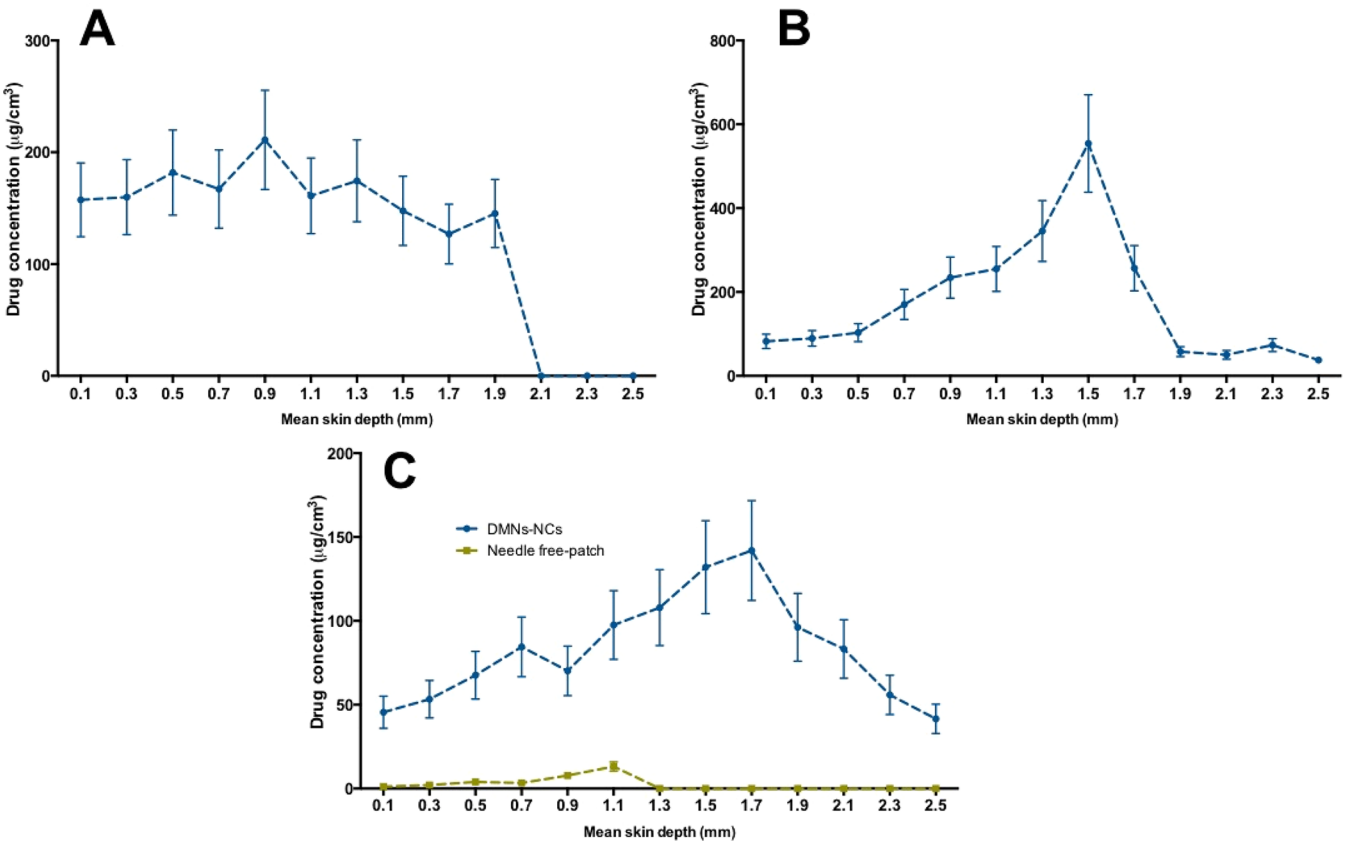

Figure 10. ABZ concentrations localized in the different layers of neonatal porcine skin, following the administration of DMNs containing ABZ-NCs at 1 h (A), t_{max} of dermatokinetic profiles (B), and 48 h (C) in comparison with needle-free patches at 48 h (3) (mean ± S.D., n = 3).

Table 2. *In Vivo* Plasma Pharmacokinetic Parameters of ABZ, ABZ-SX, and ABZ-SN Post-Oral Dosing of Coarse Suspension of ABZ and ABZ-NCs to Wistar Rats[a]

	oral-coarse suspension			oral-NCs		
parameters	ABZ	ABZ-SX	ABZ-SN	ABZ	ABZ-SX	ABZ-SN
C_{max} (μg/mL)	1.52 ± 0.42	1.38 ± 0.29	0.09 ± 0.01	2.43 ± 0.41	2.98 ± 0.51	0.12 ± 0.02
T_{max} (h)	0.5	1	4	0.5	1	2
AUC_{0-72} (h·μg/mL)	0.74 ± 0.12	13.01 ± 2.23	1.02 ± 0.23	10.84 ± 2.31	31.72 ± 6.52	2.07 ± 0.41
$AUC_{0\text{-inf}}$(h·μg/mL)	0.74 ± 0.12	14.01 ± 2.21	1.65 ± 0.28	10.95 ± 2.43	54.22 ± 8.43	3.08 ± 0.54
$T_{1/2}$ (h)	0.88 ± 0.17	13.89 ± 2.24	14.60 ± 2.73	3.54 ± 0.67	48.75 ± 8.04	33.41 ± 6.82
MRT (h)	0.68 ± 0.14	1.08 ± 0.31	9.09 ± 1.02	6.06 ± 1.32	58.03 ± 11.91	43.5 ± 7.49

[a]Mean ± SD, n = 3 for each group.

Table 3. *In Vivo* Plasma Pharmacokinetic Parameters of ABZ, ABZ-SX, and ABZ-SN Following DMNs Administration of Coarse Suspension of ABZ and ABZ-NCs to Wistar Rats[a]

	DMNs-coarse suspension			DMNs-NCs		
parameters	ABZ	ABZ-SX	ABZ-SN	ABZ	ABZ-SX	ABZ-SN
C_{max} (μg/mL)	0.29 ± 0.06	0.08 ± 0.01	0.06 ± 0.01	0.96 ± 0.32	0.32 ± 0.07	0.06 ± 0.01
T_{max} (h) had	24	24	48	6	24	48
AUC_{0-72} (h· μg/mL)	12.09 ± 1.33	2.70 ± 0.43	2.82 ± 0.66	57.59 ± 12.49	16.51 ± 3.62	2.88 ± 0.61
$AUC_{0\text{-inf}}$ (h· μg/mL)	20.56 ± 4.01	4.27 ± 0.61	N/A	189.23 ± 33.51	36.03 ± 6.09	N/A
$T_{1/2}$ (h)	43.52 ± 8.09	36.31 ± 7.19	N/A	136.18 ± 21.28	69.38 ± 10.81	N/A
MRT (h)	76.35 ± 18.81	70.31 ± 13.19	N/A	197.44 ± 34.23	110.87 ± 24.09	N/A

[a]Mean ± SD, n = 3 for each group.

were found to be 0.68 ± 0.14, 6.06 ± 1.32, 76.35 ± 18.81, and 197.44 ± 34.23 h after the oral dosing of coarse ABZ, the oral dosing of ABZ-NCs, the DMN application of coarse ABZ, and the DMN application of ABZ-NCs. After statistical analyses, the values of AUC_{0-72}, the $t_{1/2}$, and MRT of ABZ after DMN application of ABZ-NCs were determined to be statistically greater ($p < 0.05$) in comparison with postoral application. Considering these parameters, despite the lower C_{max}, the

https://doi.org/10.1021/acsami.1c11179
ACS Appl. Mater. Interfaces XXXX, XXX, XXX−XXX

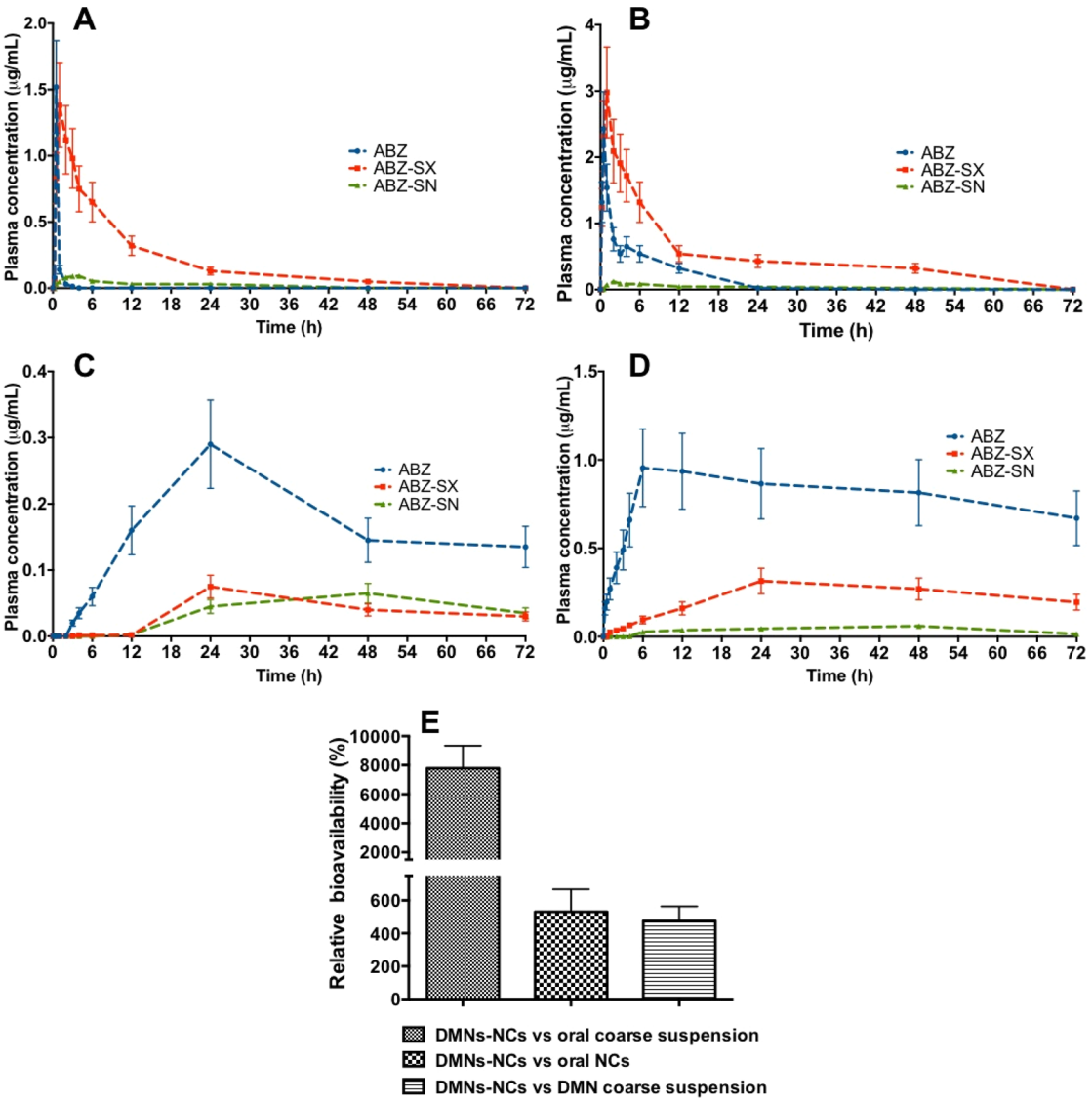

Figure 11. Mean plasma concentrations and time profiles of ABZ, ABZ-SX, and ABZ-SN after oral administration of coarse suspension of ABZ (A) and ABZ-NCs (B), as well as after intradermal administration of coarse ABZ (C) and ABZ-NCs (D) using DMNs. The relative bioavailability values of ABZ delivered by DMN-NC compared to oral administration of coarse ABZ, oral administration of ABZ-NCs, and DMN administration of ABZ-NCs (E) (mean ± SD, $n = 3$).

intradermal administration of ABZ-NCs by DMNs was able to prolong the systemic exposure of ABZ in the circulation. This may be because the release of the active substance may be sustained following the intradermal administration, leading to the longer systemic circulation.[73] The same trend has been reported earlier, showing that compared to drug administration via oral route the intradermal administration using DMNs resulted in greater AUC value.[74] It has been reported that cytochrome P450 is also found in the skin;[75] after absorption in the skin, the molecules travel in the body, including to the liver where the ABZ metabolism occurs. Additionally, the microsomes in the skin are able to metabolize known substrates of P450. In the skin, the activity of this enzyme varied between 2.5% and 13.4% of the activities in the liver. Therefore, small metabolism of ABZ through intradermal route could occur.[75,76] It was also important to note that the pharmacokinetic profiles of ABZ-SX following the oral dosing were considerably greater ($p < 0.05$) compared to the DMN administration, showing that we were able to maintain plasma concentrations of ABZ without being rapidly metabolized into ABZ-SX. Therefore, the intradermal route chosen in our study was able to avoid extensive rapid first-pass metabolism of ABZ in the liver. Without being formulated into NCs, the *in vivo* delivery of ABZ using DMNs was found to be relatively poor. The pharmacokinetic parameter values were observed to be drastically smaller ($p < 0.05$) in comparison with all cohorts in this study. This might be caused by the high deposition of ABZ in the skin. Because of its hydrophobicity, the release of ABZ in the skin was expected to be slow. This was supported by our *in vitro* release discussed previously, showing the slow release profile of ABZ compared to ABZ-NCs. Therefore, the formulation of ABZ into NCs successfully improved the *in vivo* delivery of ABZ into the systemic circulation.

In addition, by comparing the AUC values we calculated the relative bioavailability of ABZ following intradermal delivery via DMNs compared to the administration of both NCs and coarse forms via oral route. The results showed that the relative bioavailability values of ABZ delivered by DMN-NC were

https://doi.org/10.1021/acsami.1c11179
ACS Appl. Mater. Interfaces XXXX, XXX, XXX−XXX

found to be 7780.33 ± 1562.30%, 531.16 ± 136.11%, and 476.35 ± 87.11% when compared to oral administration of coarse ABZ, oral administration of ABZ-NCs, and DMN administration of ABZ-NCs, respectively. The relative biovailabilities of ABZ in DMNs-NCs cohort compared to all cohorts were more than 100%, implying the higher bioavailability of ABZ after NCs formulation delivered by DMNs. These *in vivo* studies showed that the formulation of ABZ into NCs incorporated into DMNs provide two benefits. First, the combination of NCs and DMNs could potentially enhance the bioavailability of ABZ. Second, this combination approach was able to avoid the metabolism of ABZ, which could potentially increase the effectiveness of ABZ in the treatment of CE.

According to the results discussed here, the incorporation of the NCs into DMNs was able to improve the bioavailability of ABZ, while avoiding the liver metabolism, as compared to the oral administration. Being delivered by DMNs, this technology is a safe handling, self-administered, painless, and the most suitable option for CE treatment, especially the situation where it is extremely challenging to find a healthcare professional to treat this specific disease. Therefore, it is hypothesized that this novel approach could be beneficial as an alternative treatment of CE. The preclinical efficacy of ABZ-NCs in the animal model of CE and NCs was evaluated previously using an oral treatment,[77] attaining an enhanced but limited therapeutic response against the parasite in chemoprophylaxis (which represents the rupture of the cysts during an extraction surgery) and postinfection (once the infection develops and the treatment is given) experiments.[77] Solid dispersions of ABZ were also analyzed in the same model[78] and lipid nanoparticles.[22] However, all the formulations showed limited efficacy in the CE model. In our study, as discussed previously, we were able to maintain the parent molecule in the circulation for the first time to the best of our knowledge. Therefore, we hypothesize that our findings represent a promising alternative to the current therapy of CE. However, further experiments should be considered, including toxicity studies, biocompatibility studies, and an *in vivo* pharmacodynamic study to assess the effectiveness of this novel approach in the treatment of CE.

4. CONCLUSION

This extensive work has shown the effectiveness of the combination of NCs and DMNs to overcome the issues of ABZ to potentially improve the treatment of CE. The formulation of ABZ into NCs, stabilized with Pluronic F127, enhanced the dissolution rate of ABZ, while maintaining the crystallinity of the drug. Moreover, the formulation of ABZ-NCs into DMNs with adequate mechanical properties and skin insertion abilities resulted in the enhancement of the concentration of ABZ retained in the dermis layer of the skin. Finally, plasma pharmacokinetic assessment demonstrated that the intradermal delivery of ABZ-NCs delivered by DMNs could increase the relative bioavailability of the parent drug ABZ and decrease the concentration of its metabolites, namely ABZ-SX and ABZ-SN, in comparison with the administration of coarse ABZ and ABZ-NCs via oral route, as well as DMN dosing of coarse ABZ. Therefore, this innovative approach could potentially lead to improvement of CE treatment. To prove its efficacy in the CE treatment, *in vivo* pharmacodynamic study will now be our next step.

AUTHOR INFORMATION

Corresponding Author

Ryan F. Donnelly − *School of Pharmacy, Queen's University Belfast, Belfast BT9 7BL, United Kingdom;* orcid.org/0000-0002-0766-4147; Email: r.donnelly@qub.ac.uk

Authors

Andi Dian Permana − *Department of Pharmaceutics, Faculty of Pharmacy, Hasanuddin University, Makassar 90245, Indonesia;* orcid.org/0000-0003-2168-1688

Alejandro J. Paredes − *School of Pharmacy, Queen's University Belfast, Belfast BT9 7BL, United Kingdom;* orcid.org/0000-0002-0414-8972

Fabiana Volpe Zanutto − *School of Pharmacy, Queen's University Belfast, Belfast BT9 7BL, United Kingdom; Faculty of Pharmaceutical Sciences, University of Campinas, Campinas, SP 13083-871, Brazil*

Muh. Nur Amir − *Department of Pharmacology and Toxicology, Faculty of Pharmacy, Universitas Hasanuddin, Makassar 90245, Indonesia*

Ismail Ismail − *Department of Phytochemistry, Faculty of Pharmacy, Universitas Hasanuddin, Makassar 90245, Indonesia*

Muh. Akbar Bahar − *Department of Pharmacology and Toxicology, Faculty of Pharmacy, Universitas Hasanuddin, Makassar 90245, Indonesia*

Sumarheni − *Department of Clinical Pharmacy, Faculty of Pharmacy, Universitas Hasanuddin, Makassar 90245, Indonesia*

Santiago Daniel Palma − *Unidad de Investigación y Desarrollo en Tecnología Farmacéutica (UNITEFA), CONICET and Departamento de Ciencias Farmacéuticas, Facultad de Ciencias Químicas, Universidad Nacional de Córdoba, X5000XHUA Córdoba, Argentina*

Complete contact information is available at: https://pubs.acs.org/10.1021/acsami.1c11179

Author Contributions

The manuscript was written through contributions of all authors. All authors have given approval to the final version of the manuscript

Notes

The authors declare no competing financial interest.

ACKNOWLEDGMENTS

This work was supported in part by Wellcome Trust Grant WT094085MA. The authors also thank Mrs. Dewi Primayanti for her support with the analysis of *in vivo* samples.

REFERENCES

(1) Velasco-Tirado, V.; Alonso-Sardon, M.; Lopez-Bernus, A.; Romero-Alegria, A.; Burguillo, F. J.; Muro, A.; Carpio-Perez, A.; Munoz Bellido, J. L.; Pardo-Lledias, J.; Cordero, M.; Belhassen-Garcia, M. Medical treatment of cystic echinococcosis: systematic review and meta-analysis. *BMC Infect. Dis.* **2018**, *18* (1), 1−19.

(2) Woolsey, I. D.; Miller, A. L. Echinococcus Granulosus Sensu Lato and Echinococcus Multilocularis: A Review. *Res. Vet. Sci.* **2021**, *135*, 517−522.

(3) Mandal, S.; Deb Mandal, M. Human Cystic Echinococcosis: Epidemiologic, Zoonotic, Clinical, Diagnostic and Therapeutic Aspects. Asian Pac. *Asian Pac. J. Trop. Med.* **2012**, *5* (4), 253−260.

(4) Deplazes, P.; Rinaldi, L.; Alvarez Rojas, C. A.; Torgerson, P. R.; Harandi, M. F.; Romig, T.; Antolova, D.; Schurer, J. M.; Lahmar, S.;

Cringoli, G.; Magambo, J.; Thompson, R. C. A.; Jenkins, E. J. Global Distribution of Alveolar and Cystic Echinococcosis. *Adv. Parasitol.* **2017**, *95*, 315−493.
(5) Labsi, M.; Soufli, I.; Khelifi, L.; Amir, Z. C.; Touil-Boukoffa, C. A Preventive Effect of the Combination of Albendazole and Pomegranate Peel Aqueous Extract Treatment in Cystic Echinococcosis Mice Model: An Alternative Approach. *Acta Trop.* **2019**, *197* (May), 105050.
(6) Zhang, W.; Wen, H.; Li, J.; Lin, R.; McManus, D. P. Immunology and Immunodiagnosis of Cystic Echinococcosis: An Update. *Clin. Dev. Immunol.* **2012**, *2012*, 1.
(7) Butt, A.; Khan, J. The Maverick Disease: Cystic Echinococcosis in Unusual Locations: A Ten Year Experience from an Endemic Region. *Cureus* **2019**, *11* (10), e5939 DOI: 10.7759/cureus.5939.
(8) Khan, A.; Ahmed, H.; Khan, H.; Saleem, S.; Simsek, S.; Brunetti, E.; Afzal, M. S.; Manciulli, T.; Budke, C. M. Cystic Echinococcosis in Pakistan: A Review of Reported Cases, Diagnosis, and Management. *Acta Trop.* **2020**, *212*, 105709.
(9) Larrieu, E.; Uchiumi, L.; Salvitti, J. C.; Sobrino, M.; Panomarenko, O.; Tissot, H.; Mercapide, C. H.; Sustercic, J.; Arezo, M.; Mujica, G.; Herrero, E.; Labanchi, J. L.; Grizmado, C.; Araya, D.; Talmon, G.; Galvan, J. M.; Sepulveda, L.; Seleiman, M.; Cornejo, T.; Echenique, H.; Del Carpio, M. Epidemiology, Diagnosis, Treatment and Follow-up of Cystic Echinococcosis in Asymptomatic Carriers. *Trans. R. Soc. Trop. Med. Hyg.* **2019**, *113* (2), 74−80.
(10) Brunetti, E.; Kern, P.; Vuitton, D. A. Expert Consensus for the Diagnosis and Treatment of Cystic and Alveolar Echinococcosis in Humans. *Acta Trop.* **2010**, *114* (1), 1−16.
(11) Moro, P.; Schantz, P. M. Echinococcosis: A Review. *Int. J. Infect. Dis.* **2009**, *13* (2), 125−133.
(12) Atayi, Z.; Borji, H.; Moazeni, M.; Saboor Darbandi, M.; Heidarpour, M. Zataria Multiflora Would Attenuate the Hepatotoxicity of Long-Term Albendazole Treatment in Mice with Cystic Echinococcosis. *Parasitol. Int.* **2018**, *67* (2), 184−187.
(13) Walker, M.; Rossignol, J. F.; Torgerson, P.; Hemphill, A. In Vitro Effects of Nitazoxanide on Echinococcus Granulosus Protoscoleces and Metacestodes. *J. Antimicrob. Chemother.* **2004**, *54* (3), 609−616.
(14) Chai, J.; Menghebat; Wei, J.; Deyu, S.; Bin, L.; Jincao, S.; Chen, F.; Xiong, L.; Yiding, M.; Xiuling, W.; Dolikun; Guliber; Yanchun, W.; Fanghua, G.; Shuhua, X. Observations on Clinical Efficacy of Albendazole Emulsion in 264 Cases of Hepatic Cystic Echinococcosis. *Parasitol. Int.* **2004**, *53* (1), 3−10.
(15) Martin, R. J. Modes of Action of Anthelmintic Drugs. *Vet. J.* **1997**, *154* (1), 11−34.
(16) Alanazi, F. K.; El-Badry, M.; Ahmed, M. O.; Alsarra, I. A. Improvement of Albendazole Dissolution by Preparing Microparticles Using Spray-Drying Technique. *Sci. Pharm.* **2007**, *75* (2), 63−79.
(17) Simonazzi, A.; Cid, A. G.; Paredes, A. J.; Schofs, L.; Gonzo, E. E.; Palma, S. D.; Bermúdez, J. M. Development and in Vitro Evaluation of Solid Dispersions as Strategy to Improve Albendazole Biopharmaceutical Behavior. *Ther. Delivery* **2018**, *9* (9), 623−638.
(18) Mingjie, W.; Shuhua, X.; Junjie, C.; Bin, L.; Cheng, F.; Weixia, S.; Hotez, P. Albendazole−Soybean Oil Emulsion for the Treatment of Human Cystic Echinococcosis: Evaluation of Bioavailability and Bioequivalence. *Acta Trop.* **2002**, *83* (2), 177−181.
(19) García, J. J.; Bolás, F.; Torrado, J. J. Bioavailability and Efficacy Characteristics of Two Different Oral Liquid Formulations of Albendazole. *Int. J. Pharm.* **2003**, *250* (2), 351−358.
(20) Vogt, M.; Kunath, K.; Dressman, J. B. Dissolution Improvement of Four Poorly Water Soluble Drugs by Cogrinding with Commonly Used Excipients. *Eur. J. Pharm. Biopharm.* **2008**, *68*, 330−337.
(21) Wen, H.; New, R. R.; Muhmut, M.; Wang, J. H.; Wang, Y. H.; Zhang, J. H.; Shao, Y. M.; Craig, P. S. Pharmacology and Efficacy of Liposome-Entrapped Albendazole in Experimental Secondary Alveolar Echinococcosis and Effect of Co-Administration with Cimetidine. *Parasitology* **1996**, *113*, 111−121.
(22) Pensel, P. E.; Ullio Gamboa, G.; Fabbri, J.; Ceballos, L.; Sanchez Bruni, S.; Alvarez, L. I.; Allemandi, D.; Benoit, J. P.; Palma, S. D.; Elissondo, M. C. Cystic Echinococcosis Therapy: Albendazole-Loaded Lipid Nanocapsules Enhance the Oral Bioavailability and Efficacy in Experimentally Infected Mice. *Acta Trop.* **2015**, *152*, 185−194.
(23) Abulaihaiti, M.; Wu, X.-W.; Qiao, L.; Lv, H.-L.; Zhang, H.-W.; Aduwayi, N.; Wang, Y.-J.; Wang, X.-C.; Peng, X.-Y. Efficacy of Albendazole-Chitosan Microsphere-Based Treatment for Alveolar Echinococcosis in Mice. *PLoS Neglected Trop. Dis.* **2015**, *9*, e0003950.
(24) Paredes, A. J.; Llabot, J. M.; Sánchez Bruni, S.; Allemandi, D.; Palma, S. D. Self-Dispersible Nanocrystals of Albendazole Produced by High Pressure Homogenization and Spray-Drying. *Drug Dev. Ind. Pharm.* **2016**, *42* (10), 1564−1570.
(25) Paredes, A. J.; Bruni, S. S.; Allemandi, D.; Lanusse, C.; Palma, S. D. Albendazole Nanocrystals with Improved Pharmacokinetic Performance in Mice. *Ther. Delivery* **2018**, *9* (2), 89−97.
(26) Paredes, A. J.; Litterio, N.; Dib, A.; Allemandi, D. A.; Lanusse, C.; Bruni, S. S.; Palma, S. D. A Nanocrystal-Based Formulation Improves the Pharmacokinetic Performance and Therapeutic Response of Albendazole in Dogs. *J. Pharm. Pharmacol.* **2017**, *70* (1), 51−58.
(27) Permana, A. D.; Tekko, I. A.; McCrudden, M. T. C.; Anjani, Q. K.; Ramadon, D.; McCarthy, H. O.; Donnelly, R. F. Solid Lipid Nanoparticle-Based Dissolving Microneedles: A Promising Intradermal Lymph Targeting Drug Delivery System with Potential for Enhanced Treatment of Lymphatic Filariasis. *J. Controlled Release* **2019**, *316*, 34−52.
(28) Lopez-Garcia, M. L.; Torrado-Duran, S.; Torrado-Duran, J.; Martínez-Fernández, A. R.; Bolás-Fernández, F. Albendazole versus Ricobendazole (Albendazole-Sulfoxide) against Enteral and Parenteral Stages of Trichinella Spiralis in Mice. *Int. J. Parasitol.* **1997**, *27* (7), 781−785.
(29) Daniel-Mwuambete, K.; Ponce-Gordo, F.; Torrado, J.; Torrado, S.; Cuesta-Bandera, C. Effect of Two Formulations of Benzimidazole Carbamates on The Viability of Cysts of Enchinococcus Granulosus In. *Vivo. Parasite* **2003**, *10*, 371−373.
(30) Qindeel, M.; Ullah, M. H.; Fakhar-ud-Din; Ahmed, N.; Rehman, A. ur Recent Trends, Challenges and Future Outlook of Transdermal Drug Delivery Systems for Rheumatoid Arthritis Therapy. *J. Controlled Release* **2020**, *327*, 595−615.
(31) Ramadon, D.; McCrudden, M. T. C.; Courtenay, A. J.; Donnelly, R. F. Enhancement Strategies for Transdermal Drug Delivery Systems: Current Trends and Applications. *Drug Delivery Transl. Res.* **2021**, 0123456789.
(32) Permana, A. D.; McCrudden, M. T. C.; Donnelly, R. F. Enhanced Intradermal Delivery of Nanosuspensions of Antifilariasis Drugs Using Dissolving Microneedles: A Proof of Concept Study. *Pharmaceutics* **2019**, *11* (7), 346.
(33) Permana, A. D.; Mir, M.; Utomo, E.; Donnelly, R. F. Bacterially Sensitive Nanoparticle-Based Dissolving Microneedles of Doxycycline for Enhanced Treatment of Bacterial Biofilm Skin Infection: A Proof of Concept Study. *Int. J. Pharm. X* **2020**, *2*, 100047.
(34) Paredes, A. J.; Ramöller, I. K.; McKenna, P. E.; Abbate, M. T. A.; Volpe-Zanutto, F.; Vora, L. K.; Kilbourne-Brook, M.; Jarrahian, C.; Moffatt, K.; Zhang, C.; Tekko, I. A.; Donnelly, R. F. Microarray Patches: Breaking down the Barriers to Contraceptive Care and HIV Prevention for Women across the Globe. *Adv. Drug Delivery Rev.* **2021**, *173*, 331−348.
(35) Raghava Srivalli, K. M.; Mishra, B. M.; Mishra, B. Drug Nanocrystals: A Way toward Scale-Up. *Saudi Pharm. J.* **2016**, *24* (4), 386−404.
(36) Mohammad, I. S.; Hu, H.; Yin, L.; He, W. Drug Nanocrystals: Fabrication Methods and Promising Therapeutic Applications. *Int. J. Pharm.* **2019**, *562*, 187−202.
(37) Keck, C. M.; Müller, R. H. Drug Nanocrystals of Poorly Soluble Drugs Produced by High Pressure Homogenisation. *Eur. J. Pharm. Biopharm.* **2006**, *62*, 3−16.

https://doi.org/10.1021/acsami.1c11179
ACS Appl. Mater. Interfaces XXXX, XXX, XXX−XXX

(38) Mauludin, R.; Müller, R. H.; Keck, C. M. Development of an Oral Rutin Nanocrystal Formulation. *Int. J. Pharm.* **2009**, *370*, 202−209.
(39) Pelikh, O.; Eckert, R. W.; Pinnapireddy, S. R.; Keck, C. M. Hair Follicle Targeting with Curcumin Nanocrystals: Influence of the Formulation Properties on the Penetration Efficacy. *J. Controlled Release* **2021**, *329*, 598−613.
(40) Shi, C.; Ignjatovic, J.; Liu, T.; Han, M.; Cun, D.; Đuris, J.; Yang, M.; Cvijic, S. In Vitro - in Vivo - in Silico Approach in the Development of Inhaled Drug Products: Nanocrystal-Based Formulations with Budesonide as a Model Drug. *Asian J. Pharm. Sci.* **2021**, *16* (xxxx), 1−13.
(41) Permana, A. D.; Nurul, R.; Layadi, P.; Himawan, A.; Juniarti, N.; Kurnia, Q.; Utomo, E.; Aulia, S.; Arjuna, A.; Donnelly, R. F. Thermosensitive and Mucoadhesive in Situ Ocular Gel for Effective Local Delivery and Antifungal Activity of Itraconazole Nanocrystal in the Treatment of Fungal Keratitis. *Int. J. Pharm.* **2021**, *602* (March), 120623.
(42) Pyo, S. M.; Hespeler, D.; Keck, C. M.; Müller, R. H. Dermal Miconazole Nitrate Nanocrystals − Formulation Development, Increased Antifungal Efficacy & Skin Penetration. *Int. J. Pharm.* **2017**, *531* (1), 350−359.
(43) Camiletti, B. X.; Camacho, N. M.; Paredes, A. J.; Allemandi, D. A.; Palma, S. D.; Grosso, N. Self-Dispersible Nanocrystals of Azoxystrobin and Cyproconazole with Increased Efficacy against Soilborne Fungal Pathogens Isolated from Peanut Crops. *Powder Technol.* **2020**, *372*, 455−465.
(44) Paredes, A. J.; McKenna, P. E.; Ramöller, I. K.; Naser, Y. A.; Volpe-Zanutto, F.; Li, M.; Abbate, M. T. A.; Zhao, L.; Zhang, C.; Abu-Ershaid, J. M.; Dai, X.; Donnelly, R. F. Microarray Patches: Poking a Hole in the Challenges Faced When Delivering Poorly Soluble Drugs. *Adv. Funct. Mater.* **2021**, *31*, 2005792.
(45) Romero, G. B.; Keck, C. M.; Müller, R. H. Simple Low-Cost Miniaturization Approach for Pharmaceutical Nanocrystals Production. *Int. J. Pharm.* **2016**, *501*, 236−244.
(46) Mir, M.; Ahmed, N.; Permana, A. D.; Rodgers, A. M.; Donnelly, R. F.; Rehman, A. U. Enhancement in Site-Specific Delivery of Carvacrol against Methicillin Resistant Staphylococcus Aureus Induced Skin Infections Using Enzyme Responsive Nanoparticles: A Proof of Concept Study. *Pharmaceutics* **2019**, *11* (11), 606.
(47) Cordeiro, A. S.; Tekko, I. A.; Jomaa, M. H.; Vora, L.; McAlister, E.; Volpe-Zanutto, F.; Nethery, M.; Baine, P. T.; Mitchell, N.; McNeill, D. W.; Donnelly, R. F. Two-Photon Polymerisation 3D Printing of Microneedle Array Templates with Versatile Designs: Application in the Development of Polymeric Drug Delivery Systems. *Pharm. Res.* **2020**, *37* (174), 1−15.
(48) Permana, A. D.; Paredes, A. J.; Volpe-Zanutto, F.; Anjani, Q. K.; Utomo, E.; Donnelly, R. F. Dissolving Microneedle-Mediated Dermal Delivery of Itraconazole Nanocrystals for Improved Treatment of Cutaneous Candidiasis. *Eur. J. Pharm. Biopharm.* **2020**, *154* (July), 50−61.
(49) Permana, A. D.; Anjani, Q. K.; Sartini; Utomo, E.; Volpe-Zanutto, F.; Paredes, A. J.; Evary, Y. M.; Mardikasari, S. A.; Pratama, M. R.; Tuany, I. N.; Donnelly, R. F. Selective Delivery of Silver Nanoparticles for Improved Treatment of Biofilm Skin Infection Using Bacteria-Responsive Microparticles Loaded into Dissolving Microneedles. *Mater. Sci. Eng., C* **2021**, *120*, 111786.
(50) González-Vázquez, P.; Larrañeta, E.; McCrudden, M. T. C.; Jarrahian, C.; Rein-Weston, A.; Quintanar-Solares, M.; Zehrung, D.; McCarthy, H.; Courtenay, A. J.; Donnelly, R. F. Transdermal Delivery of Gentamicin Using Dissolving Microneedle Arrays for Potential Treatment of Neonatal Sepsis. *J. Controlled Release* **2017**, *265* (1), 30−40.
(51) McCrudden, M. T. C.; Larrañeta, E.; Clark, A.; Jarrahian, C.; Rein-Weston, A.; Lachau-Durand, S.; Niemeijer, N.; Williams, P.; Haeck, C.; McCarthy, H. O.; Zehrung, D.; Donnelly, R. F. Design, Formulation and Evaluation of Novel Dissolving Microarray Patches Containing a Long-Acting Rilpivirine Nanosuspension. *J. Controlled Release* **2018**, *292* (7), 119−129.
(52) Zhang, Y.; Huo, M.; Zhou, J.; Xie, S. PKSolver: An Add-in Program for Pharmacokinetic and Pharmacodynamic Data Analysis in Microsoft Excel. *Comput. Methods Programs Biomed.* **2010**, *99* (9), 306−314.
(53) Paredes, A. J.; Camacho, N. M.; Schofs, L.; Dib, A.; Zarazaga, M. d. P.; Litterio, N.; Allemandi, D. A.; Sanchez Bruni, S.; Lanusse, C.; Palma, S. D. Ricobendazole Nanocrystals Obtained by Media Milling and Spray Drying: Pharmacokinetic Comparison with the Micronized Form of the Drug. *Int. J. Pharm.* **2020**, *585*, 119501.
(54) Melian, M. E.; Paredes, A.; Munguía, B.; Colobbio, M.; Ramos, J. C.; Teixeira, R.; Manta, E.; Palma, S.; Faccio, R.; Domínguez, L. Nanocrystals of Novel Valerolactam-Fenbendazole Hybrid with Improved in Vitro Dissolution Performance. *AAPS PharmSciTech* **2020**, *21* (7), 237 DOI: 10.1208/s12249-020-01777-y.
(55) Keck, C. M.; Müller, R. H. Size Analysis of Submicron Particles by Laser Diffractometry−90% of the Published Measurements Are False. *Int. J. Pharm.* **2008**, *355* (1−2), 150−163.
(56) Van Eerdenbrugh, B.; Van den Mooter, G.; Augustijns, P. Top-down Production of Drug Nanocrystals: Nanosuspension Stabilization, Miniaturization and Transformation into Solid Products. *Int. J. Pharm.* **2008**, *364*, 64.
(57) Liu, P.; Rong, X.; Laru, J.; Van Veen, B.; Kiesvaara, J.; Hirvonen, J.; Laaksonen, T.; Peltonen, L. Nanosuspensions of Poorly Soluble Drugs: Preparation and Development by Wet Milling. *Int. J. Pharm.* **2011**, *411* (1−2), 215−222.
(58) Abdelbary, A. A.; Al-Mahallawi, A. M.; Abdelrahim, M. E.; Ali, A. M. A. Preparation, Optimization, and in Vitro Simulated Inhalation Delivery of Carvedilol Nanoparticles Loaded on a Coarse Carrier Intended for Pulmonary Administration. *Int. J. Nanomed.* **2015**, *10* (1), 6339−6353.
(59) Permana, A. D.; Utami, R. N.; Courtenay, A. J.; Manggau, M. A.; Donnelly, R. F.; Rahman, L. Phytosomal Nanocarriers as Platforms for Improved Delivery of Natural Antioxidant and Photoprotective Compounds in Propolis: An Approach for Enhanced Both Dissolution Behaviour in Biorelevant Media and Skin Retention Profiles. *J. Photochem. Photobiol., B* **2020**, *205*, 111846.
(60) Dash, S.; Murthy, P. N.; Nath, L.; Chowdhury, P. Kinetic Modelling on Drug Release from Controlled Drug Delivery Systems. *Acta Polym. Pharm. - Drug Res.* **2010**, *67* (3), 217−223.
(61) Ramöller, I. K.; Tekko, I. A.; McCarthy, H. O.; Donnelly, R. F. Rapidly Dissolving Bilayer Microneedle Arrays − A Minimally Invasive Transdermal Drug Delivery System for Vitamin B12. *Int. J. Pharm.* **2019**, *566*, 299−306.
(62) Larrañeta, E.; Moore, J.; Vicente-Pérez, E. M.; González-Vázquez, P.; Lutton, R.; Woolfson, A. D.; Donnelly, R. F. A Proposed Model Membrane and Test Method for Microneedle Insertion Studies. *Int. J. Pharm.* **2014**, *472*, 65−73.
(63) McCrudden, M. T. C.; Alkilani, A. Z.; McCrudden, C. M.; McAlister, E.; McCarthy, H. O.; Woolfson, A. D.; Donnelly, R. F. Design and Physicochemical Characterisation of Novel Dissolving Polymeric Microneedle Arrays for Transdermal Delivery of High Dose, Low Molecular Weight Drugs. *J. Controlled Release* **2014**, *180* (1), 71−80.
(64) Donnelly, R. F.; Moffatt, K.; Alkilani, A. Z.; Vicente-Perez, E. M.; Barry, J.; McCrudden, M. T. C.; Woolfson, A. D. Hydrogel-Forming Microneedle Arrays Can Be Effectively Inserted in Skin by Self-Application : A Pilot Study Centred on Pharmacist Intervention and a Patient Information Leaflet. *Pharm. Res.* **2014**, *31* (8), 1989−1999.
(65) Donnelly, R. F.; Garland, M. J.; Morrow, D. I.J.; Migalska, K.; Singh, T. R. R.; Majithiya, R.; Woolfson, A. D. Optical Coherence Tomography Is a Valuable Tool in the Study of the Effects of Microneedle Geometry on Skin Penetration Characteristics and In-Skin Dissolution. *J. Controlled Release* **2010**, *147* (3), 333−341.
(66) Lutton, R. E. M.; Larrañeta, E.; Kearney, M. C.; Boyd, P.; Woolfson, A. D.; Donnelly, R. F. A Novel Scalable Manufacturing Process for the Production of Hydrogel-Forming Microneedle Arrays. *Int. J. Pharm.* **2015**, *494* (1), 417−429.

https://doi.org/10.1021/acsami.1c11179
ACS Appl. Mater. Interfaces XXXX, XXX, XXX−XXX

(67) Vora, L. K.; Vavia, P. R.; Larrañeta, E.; Bell, S. E. J.; Donnelly, R. F. Novel Nanosuspension-Based Dissolving Microneedle Arrays for Transdermal Delivery of a Hydrophobic Drug. *J. Interdiscip. Nanomedicine* **2018**, *3* (2), 89−101.
(68) Volpe-Zanutto, F.; Ferreira, L.; Permana, A. D.; Kirkby, M.; Paredes, A. J.; Vora, L.; Bonfanti, A.; Charlie-Silva, I.; Raposo, C.; Figueiredo, M. C.; Souza, I. M. O.; Brisibe, A.; Costa, F. D.; Donnelly, R. F.; Foglio, M. A. Artemether and Lumefantrine Dissolving Microneedle Patches with Improved Pharmacokinetic Performance and Antimalarial Efficacy in Mice Infected with Plasmodium Yoelii. *J. Controlled Release* **2021**, *333*, 298−315.
(69) Permana, A. D.; Nainu, F.; Moffatt, K.; Larrañeta, E.; Donnelly, R. F. Recent Advances in Combination of Microneedles and Nanomedicines for Lymphatic Targeted Drug Delivery. *Wiley Interdiscip. Rev.: Nanomed. Nanobiotechnol.* **2021**, *13*, 1−22.
(70) Hinderliter, P.; Saghir, S. A. *Pharmacokinetics. Encycl. Toxicol. Third Ed.* **2014**, *87*, 849−855.
(71) Pirmohamed, M. Pharmacogenetics for the Prescriber. Med. *United Kingdom* **2016**, *44* (7), 412−415.
(72) Panchagnula, R.; Thomas, N. S. Biopharmaceutics and Pharmacokinetics in Drug Research. *Int. J. Pharm.* **2000**, *201* (2), 131−150.
(73) Vora, L. K.; Moffatt, K.; Tekko, I. A.; Paredes, A. J.; Volpe-Zanutto, F.; Mishra, D.; Peng, K.; Raj Singh Thakur, R.; Donnelly, R. F. Microneedle Array Systems for Long-Acting Drug Delivery. *Eur. J. Pharm. Biopharm.* **2021**, *159*, 44−76.
(74) Zhang, S.; Qin, G.; Wu, Y.; Gao, Y.; Qiu, Y.; Li, F.; Xu, B. Enhanced Bioavailability of L-Carnitine after Painless Intradermal Delivery vs. Oral Administration in Rats. *Pharm. Res.* **2011**, *28* (1), 117−123.
(75) Venkatesh, K.; Levi, P. E.; Inman, A. O.; Monteiro-Riviere, N. A.; Misra, R.; Hodgson, E. Enzymatic and Immunohistochemical Studies on the Role of Cytochrome P450 and the Flavin-Containing Monooxygenase of Mouse Skin in the Metabolism of Pesticides and Other Xenobiotics. *Pestic. Biochem. Physiol.* **1992**, *43* (1), 53−66.
(76) Ahmad, N.; Mukhtar, H. Cytochrome P450: A Target for Drug Development for Skin Diseases. *J. Invest. Dermatol.* **2004**, *123* (3), 417−425.
(77) Pensel, P.; Paredes, A.; Albani, C. M.; Allemandi, D.; Sanchez Bruni, S.; Palma, S. D.; Elissondo, M. C. Albendazole Nanocrystals in Experimental Alveolar Echinococcosis: Enhanced Chemoprophylactic and Clinical Efficacy in Infected Mice. *Vet. Parasitol.* **2018**, *251*, 78−84.
(78) Pensel, P. E.; Castro, S.; Allemandi, D.; Bruni, S. S.; Palma, S. D.; Elissondo, M. C. Enhanced Chemoprophylactic and Clinical Efficacy of Albendazole Formulated as Solid Dispersions in Experimental Cystic Echinococcosis. *Vet. Parasitol.* **2014**, *203* (1−2), 80−86.

https://doi.org/10.1021/acsami.1c11179
ACS Appl. Mater. Interfaces XXXX, XXX, XXX−XXX